The effect of global warming on the establishment of mangroves in coastal Louisiana during the Holocene

Erika Rodrigues[a]; Marcelo C. L. Cohen[a], Kam-biu Liu[b], Luiz C.R. Pessenda[c], Qiang Yao[b], Junghyung Ryu[b], Dilce Rossetti[d], Adriana de Souza[a], Marianne Dietz[b]

[a] Laboratory of Coastal Dynamics, Graduate Program of Geology and Geochemistry, Federal University of Pará, Brazil Federal University of Pará. Rua Augusto Corrêa, 01 - Guamá. CEP 66075-110, Belém (PA), Brazil.

[b]Department of Oceanography and Coastal Sciences, Louisiana State University, Baton Rouge, Louisiana 70803, U.S.A

[c] University of São Paulo, CENA/^{14}C Laboratory, Av. Centenário 303, 13400-000, Piracicaba, São Paulo, Brazil.

[d] National Space Research Institute (INPE), Rua dos Astronautas 1758-CP 515, CEP: 12245-970, São José dos Campos (SP), Brazil.

*Corresponding author: Marcelo Cancela Lisboa Cohen

Federal University of Pará - Brazil

Rua Augusto Corrêa, 01 - Guamá. CEP 66075-110, Belém (PA), Brazil.

Tel.: +55 91 3201-7988

E-mail address: mcohen80@hotmail.com

Abstract

Winter temperature and sea-level position are critical factors affecting the global distribution of mangroves and saltmarshes. The replacement of saltmarshes by mangroves is expected due to global warming, reflecting the long-term natural trends in the Holocene and anthropogenic impacts since the 20th century. We documented the Holocene history of wetlands dynamics in the boreal limits of the American mangroves, located at Bay Champagne, Louisiana (USA), by integrating sedimentological, palynological, geochemical ($\delta^{13}C$ and C\N), X-ray fluorescence (XRF) data, and radiocarbon chronology from two sediment cores. The results indicated a freshwater lake environment with herbs and wetland ferns, as well as C_3 terrestrial plants, between ~8100 and ~6500 cal yr BP. This environment shifted into a lagoon and saltmarshes having sedimentary organic matter sourced from marine algae between ~6500 and ~1500 cal yr BP. In the final stage, washover sediments were deposited in the lagoon during the last ~1500 cal yr BP. Despite the increased marine influence over the last ~6500 cal yr BP, mangrove pollen were not recorded between ~8100 and ~1500 cal yr BP, suggesting that mangroves were absent in the study area during that time interval. Historical evidence and a comparative analysis of our multi-proxy data with other mangrove studies from the Gulf of Mexico, Caribbean, and eastern South America revealed a gradual mangrove expansion from tropical to subtropical coasts of South and North America during the mid-late Holocene. The mangrove colonies at their current boreal (29º 09` N) and austral (28º 29´ S) limits were established in the early and mid 20th century, respectively. This mangrove dynamics on a continental scale suggests that the poleward mangrove migration was likely caused by the warming climate during the Holocene. More importantly, the industrial-era warming has likely accelerated the

mangrove expansion, but it was not the primary force that drove the mangrove migration into temperate zones.

Keywords: Anthropocene; *Avicennia*; isotopes; palynology; Port Fourchon

1.Introduction

Mangroves are perhaps some of the most typical ecosystems of tropical coasts, consisting of valuable and productive intertidal forests (Food and Agriculture Organization of the United Nations., 2007; Ribeiro et al., 2019). The main products and services of mangroves include protection from storms and sea-level rise (Alongi, 2008); plant and animal productivity (Ewel et *al.*, 1998); sources of organic matter for coastal ecosystems (Walsh and Nittrouer, 2004; Dittmar et al., 2006); and sequestration and storage of atmospheric and oceanic carbon, thereby mitigating climate change effects (Fisher and Huo, 2012; Taillardat et al., 2018).

Mangroves are also very useful indicators of climate and sea-level changes (Blasco et al., 1996; Fromard et al., 2004; Alongi, 2008) due to the high susceptibility to variations in air/water temperatures, subsidence, tidal flooding frequency, river discharge, estuarine salinity, and nutrient flux, as well as tropical cyclones intensified by climate changes (Amaral et al., 2006; McLeod and Salm, 2006; Cohen et al., 2012; Krauss et al., 2014; Liu et al., 2014; Alongi, 2015; Yao and Liu, 2017). However, depending on the latitude and proximity of large estuaries, some environmental drivers may operate more intensely in controlling the mangrove dynamics, such as winter temperatures on subtropical zones (Cohen et al., 2020b), and fluvial discharge, for instance, near the Amazon River (Cohen et al., 2012). Regarding the northern and southern limits of American mangroves, the air/water temperature becomes the most critical factor in controlling the establishment, expansion, and contraction of mangroves

74 (Cavanaugh et al., 2018; 2019). This ecosystem cannot develop under low temperatures,
75 and then they occur mainly between latitudes 25° N and 25° S (Giri et al., 2011). Its
76 distribution is limited to zones where the coldest-monthly temperature average is above
77 20°C and the annual temperature range is less than 5°C (Walsh, 1974; Chapman, 1975;
78 Duke, 1992). This restriction is associated with mangrove's low tolerance to low air
79 temperature, usually inhibiting at around 5°C (Tomlinsom, 1986; Stuart *et al*., 2007;
80 Krauss *et al*., 2014). A consequence of global warming is that mangroves can expand
81 into temperate zones. Some studies have documented the influence of changes in air
82 temperature in the latitudinal distribution of mangroves (Everitt et al., 1996; Stevens et
83 al., 2006a; Perry and Mendelssohn, 2009a; Stokes et al., 2010; Osland et al., 2015,
84 2017, 2018, 2019).

85 Records of mangrove species on Earth during the Tertiary (Sherrod and
86 McMillan, 1985) and Quaternary (Cannon et al., 2009) revealed that the climate
87 controlled their establishment and extinction in the northern hemisphere (Sun and Li,
88 1999). Mangrove dynamics is generally associated with global climate and sea-level
89 changes since the Last Glaical Maximum (LGM) (Alongi, 2008). In North America,
90 there were alternations of mangrove expansion and contraction in response to
91 pronounced changes in temperatures over the late Quaternary (Sherrod and McMillan,
92 1985; Woodroffe and Grindrod, 1991; Sandoval-Castroet al., 2012a; Saintilian et al.,
93 2014; Osland et al., 2017), and they were restricted to regions equatorward of their
94 modern limits during the LGM. During this period, mangroves also decreased in Asia
95 and Europe (Woodroffe and Grindrod, 1991; Cannon et al., 2009), being restricted to
96 refuge areas with less impact of cold air temperature (Cannon et al., 2009). However, a
97 poleward expansion was recorded in the Northern Hemisphere after 19000 years ago
98 (Sandoval-Castro *et al*., 2012b; Kennedy *et al*., 2016). In the Caribbean, mangrove

99 northern limit retreated to more equatorial zones during the Pleistocene (Sherrod and
100 McMillan, 1985). As a result of warmer climates and higher sea levels during the
101 Holocene, mangroves expanded poleward, reaching Florida (Yao and Liu, 2017), Texas
102 (Sherrod and McMillan, 1985), and Louisiana (McKee and Vervaeke, 2018) at different
103 times.

104 According to pollen and isotopic studies from the South China Sea, mangroves
105 would have replaced boreal forests and temperate grasslands due to a slight increase in
106 air temperature and slow marine transgression at ~14000 cal yr BP (Sun and Li, 1999).
107 Meanwhile, mangroves were not recorded in North America or Europe, probably due to
108 the low temperatures (Sherrod and McMillan, 1985).

109 The increased winter temperatures during the last century (IPCC, 2014), mainly
110 in boreal and temperate regions (Solomon et al., 2007), caused a mangrove expansion in
111 the Gulf of Mexico (Cavanaugh et al., 2014), resulting in the replacement of salt marsh
112 vegetation dominated by *Spartina alterniflora* (Sherrod and McMillan, 1985).

113 The ecological implications of global warming to the new biogeography of
114 ecosystems adapted to tropical areas in the near future can be studied by reconstructing
115 the long-term dynamics of mangroves, mainly along the northern and southern
116 mangrove limits in the Americas. As such, a stratigraphic analysis of mangroves
117 relative to sea-level and climate changes during the Holocene must be provided from
118 various coastal environments to permit an inter-regional comparison. This work aims to
119 discuss the influence of sea-level changes and global warming on American mangroves
120 during the Holocene. We studied the Holocene changes in coastal depositional
121 paleoenvironments, and the dynamics of temperate vegetation and mangroves in
122 southern Louisiana, USA, representing the modern boreal limit of the American
123 mangroves, by the integration of sedimentological, palynological, geochemical ($\delta^{13}C$

and C\N), X-ray fluorescence (XRF) data, and radiocarbon chronology. These data are essential to evaluate and calibrate models that predict the fate of mangroves as the minimum winter temperatures continue to increase (Cavanaugh et al., 2014; 2015; 2018).

2. Study area

2.1 Geomorphology

The Caminada-Moreau Headland is a complex mosaic of barrier islands formed by the transport of sediments by wind, waves, and tidal and longshore currents (Kulp et al., 2005). The study area in Bay Champagne (29° 6` 53, 10" N / 90° 10' 33, 38"W, Fig. 1) is located in the southwestern end of this headland, near Port Fourchon in the State of Louisiana. This site is part of the Lafourche complex delta lobes, formed ~3500 years ago, and remained active until 1600 to 600 cal yr BP. During this time, nutrient-rich sediments were deposited in floodplains along tributaries, contributing to establishing wetland systems across subdeltas (Blum and Roberts, 2012).

Bay Champagne (BC) is a semi-circular brackish lagoon (salinity: 32‰) (Fig.1b, and c), with a maximum depth of 2.5 m (Liu et al., 2011). The lagoon is surrounded by cordgrass *(Spartina alterniflora)* and black mangrove *(Avicennia germinans*) vegetation (Naquin et al., 2014a). A sandy barrier, standing ~2 m above the mean relative sea-level, partially protects the backbarrier tidal flat wetlands from the impact of high energy waves and storm-forced winds (Dietz et al., 2018). Local barrier islands, including the Timbalier Island and Grand Isle (Penland, 1988), are strongly affected by erosion due to overwashing (Liu et al., 2011; Dietz et al., 2018). In addition, the decadal historical record from Bay Champaign indicates rapid shoreline retreat and coastal erosion in this area, especially during active periods of hurricanes, exacerbating the long-term trend of coastal subsidence and land loss (Dietz et al., 2018). A re-

149 nourishment project was initiated in 2012 and completed in 2014 (Coastal Engineering
150 Consultants Inc., 2015), attempting to interrupt the rapid shoreline retreat process and
151 sustain barrier beaches along the Caminada-Moreau headland (Jafari et al., 2018).

152 The coastal region in southern Louisiana is especially vulnerable to global
153 climate change (Dietz et al., 2018; Johnson et al., 2020), resulting from the Holocene
154 sea-level rise (Kjerfve, 1994). Traditional models have indicated a sea-level 3 to 4 m
155 below present at 6,000 years BP, followed by a rise to 1.5 m below present at 5,000 BP
156 (Saucier, 1994).

157 *2.2 Physiography*

158 The climate in the study area is humid subtropical, with mean monthly temperatures
159 between 6ºC and 30ºC. The mean precipitation is about 1600 mm/year, with the wetter
160 season from June to September and the drier season from September to June (National
161 Climatic Data Center, 2018). During the last two centuries, the Louisiana coast has been
162 subjected to climatic anomalies (Mock et al., 2007; Perry and Mendelssohn, 2009b).
163 The Louisiana coast is frequently affected by severe weather phenomena, including
164 hurricanes, heavy rainfall, flooding, drought, heatwaves, and freezing events (Vega,
165 2012). Beach fronts and dunes along the Caminada coast support salinity tolerant
166 vegetation, especially graminoid such as cordgrass (*Spartina alterniflora*), sea oats
167 (*Uniola paniculata),* and bitter panicum *(Panicum amarum* var *amarum'Fourchon'*).
168 Cordgrass is found on active overwash deposits (Brantley et al., 2014). Trees and shrubs
169 are mainly represented by wax myrtle *(Myrica cerifera*), iva (*Iva imbricate*), vine
170 (*Lycium barbarum*), eastern baccharis (*Baccharis halimifolia),* and black mangroves
171 *(Avicennia germinans L.)* (Henry and Twilley, 2013). After the restoration project
172 (Coastal Engineering Consultants Inc, 2015), the Caminda coastline has been used for
173 vegetative plantations, including various native dune grass species. Data about the

174 modern American mangrove distribution were obtained at http://data.unep-
175 wcmc.org/datasets/4.

176 **3. Materials and methods**

177 *3.1. Remote sensing*

178 The spatial analysis was developed with high-resolution images obtained by the drone
179 Phantom 4 Advanced DJI. This drone had a FC 6310 digital 4K/20MP (RGB), which
180 provided images of high spatial resolution (2.6 cm) of the study area. The drone images
181 were processed using the Agisoft Metashape Professional version 1.6.2 software. The
182 vegetation was visually classified by photointerpretation using various tools in the
183 Global Mapper Software 19. Details about the image processing may be obtained in
184 Cohen et al. (2020a; 2020b).
185

186 *3.2. Sampling and facies description*

187 Two sediment cores (BC81- 2,75 m, 29º 6" 53,10" N / 90º 10' 33,38"W and BC82 - 4
188 m, 29º 6" 48,88' N / 90º 10' 40,83" W) were acquired via an aluminum push corer at the
189 southern margin of the BC lagoon (Fig. 1b and 1c). The cores were measured and
190 photographed in the field and kept in a cold room (4ºC) at Louisiana State University.
191 Grain size analysis (5 cm intervals) was determined by laser diffraction in the
192 Laboratory of Chemical Oceanography of the Federal University of Pará UFPA
193 (Brazil).
194 Sedimentary features, such as color, texture, lithology, and structure, were used to
195 characterize the facies (Harper, 1984; Walker, 1992). The code of sedimentary facies
196 was based on Miall (1978). The facies, pollen, isotopes, and elemental analyses were
197 grouped into facies associations to determine a sedimentary environment (Reading,

198 1996). Cluster analysis of pollen grains supported the grouping of the facies
199 associations.

200 *3.3. LOI and XRF data*

201 Loss-on-ignition (LOI) analysis was performed at 1 cm intervals. It involved heating
202 sediment samples at 105°, 550°, and 1000°C to determine the contents of water, organic
203 matter, and carbonates, respectively. XRF analysis was performed by scanning the core
204 at 2 cm intervals using a handheld Innov-X Delta XRF. Only the major chemical
205 elements in coastal sediments (ppm) representative of marine (e.g. Br, Ca, Cl, and Sr)
206 and terrestrial (e.g. Fe, Ti, and Mn) origins were selected for this analysis (Yao et al.,
207 2015).

208 *3.4. Palynological analysis*

209 The cores were sub-sampled at intervals of 5 cm, whereby 1 cm^3 of sediment was
210 removed for pollen analysis. Before the sediment processing, one tablet of exotic
211 *Lycopodium* spores was inserted into each sample to calculate the pollen concentration
212 (grains/cm^3) and pollen accumulation rates (grains/cm^2/year). Sediment samples were
213 treated following traditional pollen analytical procedures, using hydrochloric acid,
214 hydrofluoric acid, and acetic anhydride/sulfuric acid (Fægri and Iversen1989). The
215 product of this treatment was fixed on slides in a glycerin gelatin medium. Pollen and
216 spore morphology books were used as references (McAndrews *et al*., 1973; Willard *et*
217 *al*., 2004), as well as the collections of the LSU Global Paleoecology Lab. A minimum
218 of 300 pollen grains were counted for each sample. The total pollen sum did not include
219 fern spores, algae, and foraminifers. Pollen diagrams are presented as percentages of the
220 total pollen sum. The taxa were categorized into: herbs, trees and shrubs, and aquatics.

221 Cluster analysis and pollen diagram plotting were processed by the software TILIA
222 (Version 1.7.16) (Grimm, 1990).

223 *3.5. Isotopic analysis and radiocarbon dating*

224 The isotopic composition ($\delta^{13}C$) of modern organic matter was analyzed from 134
225 samples (6-50 mg) taken at 5 cm intervals along the two cores. The stable carbon
226 isotopes were determined at the Stable Isotopes Laboratory of the Center for Nuclear
227 Energy in Agriculture (CENA/USP), using an ANCA SL2020 mass spectrometer (see
228 further details in Pessenda et al. (2004)). Five sediment samples (~2 g each) were used
229 for radiocarbon dating. The samples were physically cleaned using a microscope to
230 prevent natural contamination at ^{14}C Laboratory of CENA (Pessenda et al., 2004). The
231 organic matter was chemically processed by treating with 2% HCl at 60°C over 4h,
232 washed with distilled water, and dried (50°C) to eliminate young organic fractions
233 (fulvic and/or humic acids) and carbonates (Pessenda et al., 2010; 2012). The sediment
234 organic matter was analyzed by Accelerator Mass Spectrometry (AMS) at the ^{14}C
235 Laboratory of CENA/USP, LACUFF (Fluminense Federal University, Brazil), and
236 Center for Applied Isotope Studies (UGAMS) of the University of Georgia.
237 Radiocarbon ages are reported in years before 1950 CE (yr BP). The radiocarbon ages
238 were normalized to $\delta^{13}C$ of −25‰VPDB, and are presented in cal yr BP, with a
239 precision of 2σ (Reimer et al., 2013).

240 **4. Results**

241 *4.1. Radiocarbon ages and sedimentation rates*

242 Radiocarbon ages and sedimentation rates are provided in Table 1. The ages recorded
243 ranged from 8113 to 1470 cal yr BP (Figs. 2 and 3). Partial age inversions were
244 observed between 350 (6286 - 6454 cal yr BP) and 300 cm (6406 - 6645 cal yr BP)

(Fig. 3). It can be attributed to high sedimentation rates and/or reworking of organic remains by storms or bioturbation by benthic organisms (Pessenda et al., 2012). The sedimentation rates (0.2 to 1 mm yr^{-1}) were within the range recorded in other cores sampled from tidal flats in the Gulf of Mexico (Naquin et al., 2014b; Yao et al., 2015). The sedimentation rates in the muddy segment (400 – 170 cm) of core BC82 were lower (0.6 and 0.26 mm/y) than in the sandy intervals (170 – 0 cm) of this core (1.11 mm/yr) and core BC81 (0.77 mm/yr) (Figs. 2 and 3).

4.2. Facies description

Three facies associations were recognized in the studied cores (Figs. 4, 5, and Table 2). Facies association A consisted of massive sand (facies Sm) and massive mud (facies Mm), related to a lacustrine environment. Facies association B consisted of lenticular and flaser heterolithic bedded deposits of facies Hl and Hf, respectively, related to a lagoonal environment. Facies association C, which included massive sand (Sm), and flaser heterolithic deposits (Hf), was attributed to washovers. These environments were interpreted based on the integration of sedimentary features with pollen, isotopic, C/N, LOI, and XRF data, as described in the following.

4.2.1. Facies association A (lacustrine)

This facies association was represented by the 400 – 310 cm interval of core BC82, accumulated between ~8100 and ~6500 cal yr BP. It was characterized by massive mud (Mm) and lenticular heterolithic bedded deposits (Hl; 40 - 80% silt, 20-60% clay), ranging in color from dark brown (2.5/110Y) to dark gray (3/1 10Y). This facies association contained ~4% of carbonate and ~7% of organic matter. Two ecological groups characterized by herbaceous (25 - 65%) and tree and shrub pollen (30 - 55%)

were present. The herbaceous taxa were predominantly composed of Amaranthaceae (0-20%), Asteraceae (0-18%), Poaceae (0-12%), *Amaranthus* (0-5%), and *Artemisia* (0-4%). Arboreal taxa were mainly represented by *Pinus* (0-35%), Fagaceae (0-3%), *Betula* (0-1%), and *Quercus* (0-1%). Fern pollen mainly consisted of Polypodiaceae (Fig. 3). XRF analysis indicated the highest concentration of Fe (14 k – 20 k ppm), K (8 k – 13 k ppm), Ti (1.5 k – 2 k ppm), and Mn (370 – 800 ppm), while the values for Cl (3.5 k – 12 k ppm), Ca (5.3 k – 8.6 k ppm), Br (184 - 248 ppm), and Sr (63 - 98 ppm) were the lowest. $\delta^{13}C$ values oscillated between -24.4‰ and -22.02‰ ($\bar{x}$ = -24‰), while the C/N ratio alternated between 12 and 52 ($\bar{x}$ = 25) (Fig. 5).

4.2.2. Facies association B (lagoonal)

This facies association was evidenced in cores BC81 (270 – 170 cm) (Figs. 2 and 4), and BC82 (300 – 170 cm) (Figs. 3 and 5). The sediments were accumulated between ~6525 and ~1470 cal yr BP in core BC82 and up to ~2128 cal yr BP in core BC81. They consisted of dark gray (4/1 10Y) massive mud (Mm) and lenticular heterolithic bedded deposits (Hl; 0 - 80% sand, 15 - 80% silt, 5 - 60% clay). This facies association contained ~4% of carbonate and ~7% of organic matter. The bivalve *Rangia cuneata* was present in life position. The palynological analysis permitted the identification of three ecological groups, represented by pollen of herbs (50 – 70%), trees and shrubs (20 – 55%) and aquatic plants (2 – 10%), in addition to marine markers, such as dinoflagellate cysts and foraminifera. Herbs were mainly represented by Poaceae (0-25%), Amaranthaceae (0-14%), Asteraceae (0-6%), *Amaranthus* (0-4%), *Ambrosia* (0-4%), *Bolboschoenus* (5%), Caryophyllaceae (2%), *Spartina* (0-3%) and Chenopodiaceae (0-2%). Arboreal pollen included mainly *Pinus* (0-20%), *Quercus* (0-3%), *Betula* (0-3%), and *Alnus* (0-2%). The group of aquatic plants was predominantly

295 composed of *Typha angustifolia* (0-14%) and *Typha latifolia* (0-3%) (Figs. 2 and 3).
296 *Typha angustifolia* disperses as a reticulate, monoporate monad pollen (22.7 ± 2.6 µm)
297 (Fig. 1a and b, supplementary material), and *Typha latifolia* is reliably represented in
298 the pollen record as perforate-reticulate, tetrads pollen (25.70 ± 1.58) (Finkelstein,
299 2003; Hamdi et al., 2010; Skvarla and Larson, 1963) (Fig. 1c and d, supplementary
300 material). XRF results revealed an increasing trend in Cl (3 k– 20 k ppm) and Br (190 –
301 950 ppm) and a decreasing trend in Fe (7 k - 17.5 k ppm) and Mn (186 – 500 ppm)
302 compared to facies association A. Facies association B presented more enriched $\delta^{13}C$
303 values (~-22‰) than the facies association A (~-24‰). C/N values decreased upward
304 from ~25 to ~11 within this association (Figs. 4 and 5).
305
306 *4.2.3. Facies association C (washover)*
307 These deposits were identified in both studied cores in the interval 170 – 0 cm, formed
308 during the last ~1470 cal yr BP (170 – 0 cm) and ~2100 cal yr BP in the cores BC82
309 and BC81, respectively. The cores consisted of dark gray (4/1 10Y) flaser heterolithic
310 bedded deposits (facies Hf; 60 - 100% sand, 0-40% silt, 0- 10% clay); sandy layers were
311 cross laminated. The upper part of facies association A was characterized by massive
312 sand (Sm; 14% coarse, 73% medium, 13% fine); grain size increased gradually upward
313 in this sandy facies. Shell fragments were frequent in this association. The carbonate
314 concentration oscillated between 4 and 20%, while the organic matter decreased upward
315 from 4 to 2%. A wide range of variation was recorded for the concentrations of Ca (2.7
316 k – 130 k ppm), Sr (100 – 572 ppm), Zn (0 – 46 ppm), and Zr (44 – 422 ppm). The
317 concentration of Ti (270 – 1134 ppm), and Fe (2100 – 7200 ppm) also varied largely,
318 but with values that were lower than in facies associations A and B. $\delta^{13}C$ and C/N

319 values oscillated between -20 and -27‰ and 3 and 28, respectively. No pollen grain was
320 found in this facies association (Figs. 4 and 5).
321
322 *5.0. Discussion*
323 The sampling sites are accumulating washover sediments at present (Fig. 1b and 1c).
324 These sites were chosen due to their position in the central portion of an old lake (Fig.
325 7), with the potential to preserve the oldest lacustrine records. Depositional
326 environments with a predominance of sandy sediments are not suitable for preserving
327 pollen grains (Havinga, 1967). However, such environment may have evolved from an
328 environment with low hydrodynamic flow that was favorable for the muddy (silt and
329 clay) sedimentation (Reineck and Singh, 1980; Reading, 1996) and suitable for pollen
330 preservation, as indicated by several pollen studies in tidal flats (Behling et al., 2001;
331 2004; Cohen et al., 2005a; 2005b; 2012; 2020b, Guimarães et al., 2013; Moraes et al.,
332 2017; Ribeiro et al., 2018), fluvial flood plains (Cohen et al., 2014; 2020a; Fontes et al.,
333 2017; Lima et al., 2017; Silva et al., 2018), lagoons (Cohen et al., 2020b, 2016; Franca
334 et al., 2016), and lakes (Lara and Cohen, 2009; Smith et al., 2011; Buso Junior et al.,
335 2013). For example, oxbow lakes, developed after a channel abandonment, can be filled
336 by muddy sediments and converted into a fluvial terrace or an active channel with sandy
337 deposition (Cohen et al., 2014; Rossetti et al., 2014). In the case of the study area,
338 evidence based on facies association indicated the development of a lake (~8100 -
339 ~6500 cal yr BP), which subsequently evolved into a lagoon (6500 – 1470 cal yr BP).
340 Relatively high pollen concentrations (50 k – 200 k pollen grains/cm³, Figs. 2 and 3) in
341 the sediments from this period suggested that the land around the lake and lagoon was
342 well-vegetated. Gradually over the last ~1470 cal yr BP, this coastal lake and lagoon at

343 the coring site has been filled by washover sandy sediment, which was not conducive to
344 retention and preservation of pollen.
345
346 5.1. Depositional phases
347 5.1.1. Early Holocene (~8100 - ~6500 cal yr BP): lacustrine
348 The prevalence of muddy deposits in facies association A (i.e., basis of core BC82, 400
349 – 310 cm) indicates a low energy depositional environment, most likely a freshwater
350 lake. The $\delta^{13}C$ and C/N, ranging from -24.4 to -22.02‰ and 12 to 52 respectively,
351 recorded in these deposits support that C3 terrestrial plants were the source for the
352 sedimentary organic matter (C3 plants $\delta^{13}C$: -32‰ to -21‰ and C/N: > 12; Deines,
353 1980; Meyers, 1994; Tyson, 1995). The concentrations of K, Ti, Fe, and Mn in facies
354 association A were compatible with values recorded in environments with a high input
355 of terrestrial sourced sediment (Cuven et al., 2013; Yao et al., 2018). The presence of
356 arboreal pollen from *Pinus*, *Quercus*, Fagaceae, and *Betula*, as well as herbs (mainly
357 represented by Asteraceae and Amaranthaceae) and wetland ferns (represented by
358 Polypodiaceae), conforms with a freshwater, terrestrial setting. Altogether, these
359 characteristics are taken as evidence of a lacustrine environment for facies association
360 A. The inferred lake developed in the study area during the early Holocene when the
361 sea-level was ~8 m below the modern sea-level (Donoghue, 2011) (Fig. 7).
362
363 5.1.2. Mid-late Holocene (~6500 - ~1470 cal yr BP): lagoonal
364 This phase is recorded by facies association B, which is lithologically similar to the
365 lacustrine deposits characterized by the prevalence of muddy components (facies Mm
366 and Hl) indicating low energy environments. However, the presence of the bivalve
367 *Rangia cuneate* attests to a connection to marine waters, as this species is typical of

368 brackish water environments (Tarver, 1972; Warzocha et al., 2016). This bivalve, native
369 to the Gulf of Mexico (Benson, 2010), has often been used to indicate marine influence
370 during the Holocene (Rodriguez et al., 2004; Wakida-Kusunoki, MacKenzie, 2004).
371 Accordingly, we interpret facies association B to represent a lagoon. The slight
372 enrichment of $\delta^{13}C$ values in facies association B (~-22‰) compared to the lacustrine
373 deposits (-24‰), and the decreasing C/N values from ~25 to ~9, suggest the
374 contribution of marine organic matter ($\delta^{13}C$: -24‰ to -16‰ and C/N: < 10; Deines,
375 1980; Meyers, 1994; Tyson, 1995) (Fig. 6), as expected in a lagoon. The upward
376 increase of Cl (from 4 k to 13 k ppm) and Br (from 264 to 950 ppm) and decrease of Fe
377 (from 16 k to 11 k ppm) and Mn (from 400 to 200 ppm) are also indications of a coastal
378 environment with marine influence and lower input of terrestrial sediments. The pollen
379 assemblage, marked by the increased abundance of brackishwater herbaceaous
380 (*Bolboschoenus, Spartina*) and brackishwater aquatic (*Typha angustifolia* and *Typha*
381 *latifolia)* plants, is further consistent with the inferred lagoon environment. The aquatic
382 macrophyte cattail (*Typha*) can tolerate environments with high salinity (Hameed et al.,
383 2012; Akhtar et al., 2017) and variation in water level (Ladislas et al., 2012).
384 Paleoecological studies in brackish lagoonal deposits from Mexico also indicated the
385 establishment of *Typha* ~6000 cal yr BP (Caballero et al., 2005). In addition, the
386 occurrence of foraminifera and dinoflagellate cysts in this stratigraphic unit is further
387 evidence for a marine-influenced environment, such as a lagoon.
388
389 5.1.3. Late Holocene (last ~1470 cal yr BP): shoreline retreat
390 This phase is recorded by facies association C, whereby the muddy deposits changed
391 abruptly upward into heterolithic mud/sand and massive sand. It represents the modern
392 washover sediments that are deposited inland of a beach by overwash. Overwash is the

393 flow of water and sediment over the beach's crest that does not return to the water body.
394 Coastal overwash is mainly caused by hurricanes and winter storms along the Atlantic
395 and Gulf Coasts of the United States (Liu, 2004; Donnelly et al., 2006). This
396 sedimentary succession may reflect the gradual landward migration of sandy coastal
397 barriers due to marine transgression (Fig. 7). This interpretation is based on the
398 increased marine influence with respect to the lagoon deposits of the previous phase.
399 This is evidenced by the lower input of terrestrially-sourced sediments evidenced by the
400 decreasing trend of Ti (1700 to 400 ppm), Fe (from 12 k to 2 k ppm), and Mn (from 230
401 to 75 ppm) and strong oscillations of Ca (2 k – 129 k ppm), Cl (5.6 k – 24 k ppm), Sr
402 (100 – 572 ppm), Br (230 – 1200 ppm), Zn (0 – 46 ppm), and Zr (44 – 422 ppm). High
403 Zn and Zr values are found in the sand fraction. Then, probably, oscillations of Zn and
404 Zr values indicated phases of rock weathering carried by the action of the currents and
405 tides and deposited as beach sand. Ca, Cl, Br, and Sr are constituents of
406 biogeochemical cycling in marine systems (Yao and Liu, 2017; Joe-Wong et al., 2019).
407 The significant decrease in C/N values, from ~10 to ~6, with respect to the lagoonal
408 phase, and the $\delta^{13}C$ values, between -20‰ and -27‰, are consistent with this
409 interpretation (marine algae, $\delta^{13}C$: -24‰ to -16‰ and C/N: < 10) (Deines, 1980;
410 Meyers, 1994; Tyson, 1995) (Fig. 6). Local oscillations of these values that were
411 synchronized with Ca, Sr, Zn, and Zr peak concentrations are probably a result of storm
412 events, since this coastline is notably affected by intense hurricanes and tropical storms
413 (Dietz et al., 2018; Johnson et al., 2020).
414
415 5.2. Absence of mangrove pollen along the cores
416 The analyzed cores did not contain mangrove pollen grains, despite the dense
417 occupation of *Avicennia* trees around the lagoon nowadays. Noteworthy is that lakes,

lagoons, tidal flats, and fluvial floodplains present suitable hydrodynamic conditions for muddy sedimentation with pollen derived from plants that lived at the times the sediments were deposited. Under this situation, lagoonal and lacustrine sediments preserve pollen grains transported by wind and from the flora surrounding the lake or lagoon. The spatial representation of lagoonal or lacustrine pollen records changes according to the wind intensities and the watershed area influencing the lake or lagoon (Cohen et al., 2008; 2014). In addition, the pollen percentage of each vegetation unit is distance-weighted, where the closer to the source, the greater the pollen signal from that plant (Davis, 2000; Xu et al., 2012). Thus, pollen accumulated in lagoon or lake sediments presents a wider spatial representation of the regional flora than tidal flats sediments. Pollen rain in tidal flats, mainly occupied by dense mangrove forests, should indicate local vegetation, while open canopy tends to present a higher proportion of long distance transport pollen rain (Weng et al., 2004; Gosling et al., 2009).

Considering the pollen grains can be transported by wind and currents mainly in open areas (Brush and Brush, 1972; Solomon et al., 1982; Weng et al., 2004), it is common to record <1% pollen grains that do not represent the local vegetation during the sediment accumulation. For instance, a core taken from a marsh in southwestern Louisiana revealed one or two *Avicennia* pollen grains in the 0, 210, and 280 cm depth, probably transported by currents or hurricanes (Yao et al., 2020). By contrast, cores taken from tidal flats occupied by mixed mangroves with *Rhizophora*, *Laguncularia,* and *Avicennia* in Florida contained pollen percentages of 30 – 60% of *Rhizophora*, 5 – 20% of *Avicennia*, and 5 – 15% of *Laguncularia* (Yao et al., 2015; Yao and Liu, 2017). The lagoon and tidal flat sediments covered by *Avicennia* trees in Bay Champagne, the study area, accumulate between 6 and 9% of *Avicennia* pollen (Ryu, 2020). In Amazonian mangroves, pollen traps installed on tidal flats occupied only by *Avicennia*

443 trees present ~15% (~540 grains/cm^2/yr) of *Avicennia* pollen (Behling et al., 2001).
444 Accumulation rates of *Avicennia* pollen are also relatively elevated in a mangrove with
445 *Rhizophora* and *Avicennia* trees (average 450 grains/cm^2/yr). Even in mangroves
446 dominated by *Rhizophora*, pollen grains of *Avicennia* may be found (average 120
447 grains/cm^2/yr) (Behling et al., 2001). In addition, *Avicennia* pollen grains have been
448 found in thousands of stratigraphic pollen spectra obtained from cores sampled from the
449 American coasts with *Avicennia* trees (e.g. Cohen et al., 2005a 2005b; 2009; 2012;
450 2014; 2015; 2016, Vedel et al., 2006; Peros et al., 2007; Guimarães et al., 2011, 2013;
451 Smith et al., 2011, 2012; França et al., 2014, 2016, 2019b; Yao et al., 2015b, 2017;
452 Moraes et al., 2017; Ribeiro et al., 2018; Cordero-Oviedo et al., 2019; Jones et al.,
453 2019).

454 These data suggest that sediments accumulated in tidal flats or lagoons with
455 *Avicennia* or near *Avicennia* trees tend to have a significant *Avicennia* pollen
456 representation. Therefore, the absence of *Avicennia* pollen grains in the sedimentary
457 sequences formed during the lake (8100 – 6500 cal yr BP) and lagoon (6500 – 1470 cal
458 yr BP) phases in our cores (Figs. 2 and 3) suggests that mangroves with *Avicennia* trees
459 were absent at or near our study site during the Holocene.

460 The absence of mangroves in the modern northern limit of American mangroves
461 between ~8100 and ~1470 cal yr BP is an important finding that contributes
462 significantly to the discussions about the main forces driving the mangrove
463 establishment on the American continent during the Holocene, as well as its poleward
464 expansion in the Anthropocene (since the mid-twentieth century (Zalasiewicz et al.,
465 2018)). Nevertheless, it is necessary to assess the effects of sea-level rise on the studied
466 coastal vegetation and morphology, since the salinity gradients along the zones under

467 marine or estuarine influence need to be conducive to mangrove development (Lara
468 and Cohen, 2006).
469
470
471 5.3. American mangrove establishment controlled by sea-level
472 Mangroves colonized the distal portion of the continental shelf during the Last Glacial
473 Maximum (LGM) (~27 and ~ 20 k cal yr BP) due to the worldwide lowering of the
474 eustatic sea-level (Murray-Wallace, 2007; Cohen et al., 2014). The continental shelf
475 emerged almost completely, positioning the coastline at some sites ~100 km of its
476 current location (Nittrouer et al., 1996; Clark et al., 2009; Harris et al., 2013). After the
477 LGM low sea-level, melting ice sheets caused transgression between 16 and 4 ka in
478 many areas of southern North America (Gischler, 2015) and, probably, a landward
479 mangrove migration along the continental shelf (Cohen et al., 2012; 2014). A rapid
480 relative sea-level rise was recorded on the eastern coast of South America during the
481 early-middle Holocene. The sea-level in southeastern and northeastern Brazilian coast
482 was between 5 and 1 m above the modern sea-level, at approximately 5500 cal yr BP,
483 with a gradual fall during the middle to late Holocene (Angulo et al., 2006, 2016;
484 Caldas et al., 2006; Lorente et al., 2013; Cohen et al., 2020a). Sea-levels comparable to
485 the modern one were already reached between 6000 and 5000 cal yrs BP in the northern
486 Brazilian coast (Cohen et al., 2005b; 2012). Several works have attributed the mangrove
487 establishment in the middle Holocene along the tropical coasts to the lower rates of sea-
488 level rise or a stable sea-level in the middle Holocene (Woodroffe et al., 1985, 2015;
489 Toscano and Macintyre, 2003; Khan et al., 2017; Ribeiro et al., 2018; Cohen et al.,
490 2020a) (Fig. 8). Then, mangroves were established in the tropical Brazilian littoral at
491 ~7000 cal yr BP: Espírito Santo (19º S), Bahia (17º S), Rio Grande do Norte (5º S),

492 Pará (1º S), and Amapá (2º N) (Cohen et al., 2012; 2014; 2020a; Pessenda et al., 2012;
493 França et al., 2013, 2015; Fontes et al., 2017; Ribeiro et al., 2018).

494 Similarly, transgressive events were also recorded in the northern Gulf of
495 Mexico (Anderson and Fillon, 2004), with a high sea-level rise rate of 7.4 ± 0.7 m/ka in
496 the early Holocene, and a reduced rate of 2.3 mm/yr in the middle to late Holocene
497 (Wanless et al., 1994; Khan et al., 2017). The relative stability of modern coastal
498 systems along the Gulf of Mexico is primarily due to the stabilization of sea-level
499 approximately 6,000 years ago (Donoghue, 2011). Blum et al. (2002) proposed that the
500 middle Holocene sea-level along the Texas Gulf coast was at -9 m at ca. 7.8 ka, then
501 rose rapidly to +2 m by ca. 6.8 ka. However, according to Khan et al. (2017), the
502 relative sea-level did not exceed the present height during the Holocene, and around
503 ~6.5 ka, sea-level was at 6.2 m below the modern sea-level (Willard and Bernhardt,
504 2011). The sea-level, which was near the modern level during the middle Holocene,
505 allowed mangrove establishment in the Caribbean and Gulf of Mexico coast, a tropical
506 zone, at ~6100, ~5400, ~5300, and ~5500 cal yr BP, in Venezuela (9º N), Puerto Rico
507 (18º N), Yucatan Peninsula-Mexico (18º - 21º N) and Cuba (22º N), respectively (Peros
508 et al., 2007; Cohen et al., 2016; Aragón-Moreno et al., 2018; Montoya et al., 2019). In
509 addition, mangroves were recorded in the western Gulf of Mexico coast (20º N) at
510 ~6000 cal yr BP (Cordero-Oviedo et al., 2019).

511 In the study area (29º N), marine transgression caused the development of
512 lagoons and saltmarshes with a strong contribution of marine organic matter after ~6500
513 cal yr BP (Figs. 4, 5, 6, and 7). This sedimentary environment associated with
514 vegetation and sedimentary organic matter suggests favorable physical-chemical
515 conditions for mangrove establishment. Therefore, of the sea-level dependent factors,
516 mangroves could have been established in the study area since ~6500 cal yr BP.

However, contrasting with the tropical coasts, there was no evidence of mangrove presence around the Bay Champagne lagoon, the current northern mangrove limit, between 6500 and 1470 cal yr BP. A similar situation occurred at the southern limit of American mangroves at Laguna, southern Brazilian coast (28º 29´ S), where pollen studies also indicate the absence of mangroves during the Holocene. Mangroves were established at their current southern limit of South America only in the Anthropocene (Cohen et al., 2020b). Probably, despite the physical-chemical conditions suitable for mangrove establishment promoted by the sea-level rise, the temperature may not yet have been high enough to allow the growth of mangroves at their current northern and southern limits of American mangroves during the middle-late Holocene. In addition, biogeographic studies indicated that modern global distribution of mangroves is mainly controlled by temperature, hence being limited to tropical and subtropical regions (Lugo and Patterson-zucca, 1977; Sherrod and McMillan, 1985a; Duke et al., 1998; Stevens et al., 2006b; Stuart et al., 2007).

5.4-Mangrove establishment controlled by climate

Considering that mangroves are susceptible to changes in sea-level and climate in a millennial timescale (Chapman, 1975; Duke, 1992; Blasco, 1996; Fromard et al., 2004b; Alongi, 2008), and to local factors in a secular/decadal time scale (Moraes et al., 2017; Ribeiro et al., 2018) the (1) presence or (2) absence of mangroves along their current northern and southern limits during the Holocene is essential to identify the reasons for the mangrove expansion to more temperate zones during the recent decades. Regarding the hypothesis of the (1) continuous presence of mangroves in the current northern (29º N) and southern (28º S) boundaries of the American continent (North and South America) during the middle-late Holocene, it would indicate relative stability of relative

sea-level and climate during that period. In this case, studies that show the poleward mangrove expansion during the most recent decades (e.g. Cavanaugh et al., 2014; Saintilan et al., 2014b; Osland and Feher, 2020) could be incorrectly attributing such mangrove dynamics to allogeneic processes, for instance, global warming. Alternatively, it may be caused by autogenic mechanisms, for instance, related to the action of tides, storms, dynamics of beach-barrier, delta switching, and lateral migration of meandering fluvial channels, then creating and destroying mangrove substrates in a cyclical process with expansion and contraction phases of mangrove areas in a decadal time scale (Moraes et al., 2017). In this context, such mangrove expansion would be related to processes operated locally and intrinsic to the depositional system (Beebower, 1964; Cecil, 2013).

By contrast, the (2) absence of mangroves in their current northern and southern limits in the Holocene indicates an allogeneic process driving the mangrove expansion from tropical into temperate latitudes in a millennial time scale. In general, the geological record suggests equatorward contraction of mangroves during the LGM (Woodroffe and Grindrod, 1991; Cannon et al., 2009), when these forests occurred only in refuge areas more protected from the impact of cold air temperature (Cannon et al., 2009). In contrast, a poleward mangrove expansion occurred after the LGM (Sandoval-Castro et al., 2012a; Kennedy et al., 2016). During the early and middle Holocene, this trend may have been favored in tropical to subtropical areas by increasing the global mean surface temperature (O'ishi and Abe-Ouchi, 2011; Fig. 8).

There is a consensus about global warming between the LGM and early Holocene (Kaufman et al., 2020). However, less well understood is the climate between the mid and late Holocene (Sundqvist et al., 2014). The Antarctic Peninsula underwent an early-Holocene warm phase and stable temperatures between 9,200 and 2,500 years

567 ago (Mulvaney et al., 2012). Studies over land north of 40°N have indicated warming
568 during the middle Holocene (O'ishi and Abe-Ouchi, 2011). Other proxy records
569 indicated global cooling during the late Holocene (Marcott et al., 2013). However, with
570 no direct net contribution from the orbitally-driven insolation, the global annual mean
571 radiative forcing in the Holocene should be dominated by the retreating ice sheets and
572 rising atmospheric greenhouse gases, with both favoring a globally averaged warming
573 (Liu et al., 2014). Climate models simulate a robust global annual mean warming along
574 the Holocene, mainly in response to rising CO_2 and the retreat of ice sheets (Liu et al.,
575 2014). Other climate models suggest no change or warming during the mid-late
576 Holocene (Braconnot et al., 2007; Timm and Timmermann, 2007; Lohmann et al.,
577 2013). The increase of CO_2 and CH_4 concentrations after 7000 and 5000 years ago
578 contributed to the late Holocene warmth, prolonging the natural interglacial warmth
579 initiated by orbital variations. These mid-late Holocene greenhouse gas increases may
580 be natural or anthropogenic in origin (Ruddiman, 2003; Broecker and Stocker, 2006;
581 Kaplan et al., 2011; Ruddiman et al., 2016). A stable isotope record from ice wedges
582 from the Arctic indicated a long-term winter warming trend during the mid-late
583 Holocene (Meyer et al., 2015). $\delta^{18}O$ of planktonic foraminifera from the western
584 tropical South Atlantic Ocean on the northeast Brazilian margin showed a progressive
585 warming trend of slightly more than 1°C during the transition from the mid- to late-
586 Holocene (Santos et al., 2013). A record of Holocene sea-surface temperatures and sea-
587 ice presence from the Polar Front of the East Atlantic Southern Ocean showed late
588 Holocene warming and no abrupt Neoglacial cooling (Nielsen et al., 2004). Jomelli et
589 al. (2011) proposed Holocene warming for the eastern tropical Pacific with increased
590 atmospheric temperature and retreat of glaciers in the southern tropics in response to
591 enhanced austral summer insolation. This Holocene climate trend indicated by the

592 climate models and proxy records is consistent with the hypothesis that climate
593 warming permitted mangroves to expand from the tropics to subtropics during the mid-
594 late Holocene (Fig. 8).

595 Although the coastal stabilization or low rates of sea-level change around the
596 middle Holocene may have played a role in the establishment of northern and southern
597 American mangroves in areas located between the latitude of 20ºN and 20ºS, the
598 subtropical mangroves were established only in the mid-late Holocene in both
599 hemispheres, probably as a result of global warming that caused a poleward mangrove
600 expansion from the latitude of 20º to 29º. The mangroves in the subtropical Brazilian
601 coast were established between ~2200 cal yr BP (São Paulo, 25º S) and ~1630 cal yr BP
602 (Santa Catarina-Brazil, 26º S) (Pessenda et al., 2012; França et al., 2019), and the
603 subtropical mangroves in North America appeared after ~ 4000 cal yr BP in the
604 Everglades-Florida (25º N) (Willard and Bernhardt, 2011; Yao et al., 2015; Yao and
605 Liu, 2017; Jones et al., 2019) (Fig. 8). Regional-scale droughts may have some
606 influence in delaying the mangrove establishment in the subtropical mangroves of the
607 Everglades (Willard and Bernhardt, 2011), but global warming in the mid-late
608 Holocene must be considered as the main force favoring the mangrove expansion from
609 tropical to subtropical areas in both hemispheres.

610 Our study shows the absence of mangroves between ~8100 and ~1500 cal yr BP
611 in Port Fourchon (29º 09` N), USA. The first evidence of black mangroves in Louisiana
612 was dated at approximately 1900 AD (Lloyd and Tracy, 1901). These authors described
613 early mangrove stands short in stature (<0.6 m) growing on offshore islands, mainly in
614 Breton Sound. In addition, a historical video of the U.S. Library of Congress
615 (http://www.loc.gov/item/mp76000363) also exhibited black mangroves at the Breton
616 National Wildlife Refuge in Louisiana in 1915. Similarly, in the southern limit of the

American mangroves at Laguna, Brazil (28º 29´ S), even though physicochemical and hydrodynamic conditions were favorable for the establishment and expansion of mangroves since the middle Holocene, mangrove establishment occurred only between ~1957 and ~1986 AD (Cohen et al., 2020b). It is noteworthy that a subtropical Brazilian mangrove stand (26° S), established since ~1630 cal yr BP, contained *Rhizophora* trees only during the last decades (França et al., 2019). *Rhizophora* is less tolerant to low temperatures than *Lagungularia* and *Avicennia* (Duke et al., 1998; Quisthoudt et al., 2012). The presence of mangroves in Louisiana, even incipient and restricted to some islands since the beginning of the 20th century, suggests that this ecosystem was established only after appropriate climatic conditions were present since that time.

We propose that the establishment of *Avicennia* trees in the study area was related to the natural warming trend after the Little Ice Age (LIA). This cold climatic episode was attributed to solar activity fluctuations during the last six or seven centuries (Lean and Rind, 1999), ending between 1850 and 1890 AD (Bradley and Jones, 1992). Ongoing remote sensing work (unpublished) by Cohen and co-workers indicates a significant increase in the area and stature of Louisiana mangroves in recent decades, especially in the 21st century. Therefore, while our data suggest that a poleward mangrove migration occurred due to natural global warming during the late Holocene, the industrial-era warming must have intensified the mangrove expansion during the last few decades, when temperature increased at a higher rate in the boreal and temperate regions than in the tropics (Solomon et al., 2007).

6. Conclusions

Our integrated multi-proxy investigation based on sedimentology, ^{14}C radiocarbon dating, pollen analysis, as well as X-ray fluorescence, isotope ($\delta^{13}C$), and C\N data indicate a marine transgression at Bay Champagne, Louisiana-USA during the Holocene. This natural process changed the environment from a freshwater lake (~8100 – ~6500 cal yr BP) to a brackish water lagoon (~6500 – ~1500 cal yr BP). During the last ~1500 cal yr BP, washover sand was deposited into the lagoon due to the relative sea-level rise and hurricanes. Physicochemical and hydrodynamic conditions suitable for mangrove development occurred in the study site over the last ~6500 cal yr BP. However, mangrove pollen were not recorded in sediments between ~8100 and ~1500 cal yr BP, suggesting that mangroves were absent during the entire period. A comparative analysis of these multi-proxy data and historical records of mangrove establishment phases in the Gulf of Mexico, Caribbean, and eastern South America indicated that mangroves expanded gradually from the tropical to subtropical South and North American coasts during the mid and late Holocene. The modern boreal (29º 09` N) and austral (28º 29´ S) mangrove limits were established in the early and mid 20th century, respectively. This mangrove dynamics on a continental scale suggests that poleward mangrove migration was caused by natural Holocene global warming. The industrial-era warming must have intensified the mangrove expansion. However, the Anthropocene global warming was not a direct forcing that initiated the mangrove migration into temperate zones.

7. Acknowledgments

The authors thank the Graduate Program in Geology and Geochemistry of the Federal University of Pará. We also acknowledge the logistic support provided by the College of the Coastal and Environment of the Louisiana State University. This study was financed by the Brazilian Council for Technology and Science-CNPq (Project # 307497/2018-6), FAPESP 2017/03304-1, the U.S. National Science Foundation (NSF Project # 1759715), the Ministry of Science and Technology of the People's Republic of China (Project # 2017YFE0107400), and NOAA through the Louisiana Sea Grant (Project #2013-39).

8-References

Akhtar, N., Hameed, M., Nawaz, F., Ahmad, K.S., Hamid, A., Segovia-Salcedo, C., Shahnaz, M.M., 2017. Leaf anatomical and biochemical adaptations in Typha domingensis Pers. ecotypes for salinity tolerance. Bot. Sci. 95, 807–821. https://doi.org/10.17129/botsci.886

Alongi, D.M., 2015. The Impact of Climate Change on Mangrove Forests. Curr. Clim. Chang. Reports 1, 30–39. https://doi.org/10.1007/s40641-015-0002-x

Alongi, Daniel M., 2008. Mangrove forests: Resilience, protection from tsunamis, and responses to global climate change. Estuar. Coast. Shelf Sci. 76, 1–13. https://doi.org/10.1016/j.ecss.2007.08.024

Alongi, D. M., 2008. Mangrove forests: Resiliense, protection from tsunamis, and response to global climate change. Estuar. Coast. Shelf Sci. 76, 1–13.

Amaral, P.G.C., Ledru, M.-P., Branco, F.R., Giannini, P.C.F., 2006. Late Holocene development of a mangrove ecosystem in southeastern Brazil (Itanhaém, state of São Paulo). Palaeogeogr. Palaeoclimatol. Palaeoecol. 241, 608–620. https://doi.org/10.1016/j.palaeo.2006.04.010

Anderson, J.B., Fillon, R.H., 2004. Late Quaternary stratigraphic evolution of the northern Gulf of Mexico margin. SEPM (Society for Sedimentary Geology).

Angulo, R., Lessa, G., Souza, M., 2006. A critical review of mid- to late-Holocene sea-level fluctuations on the eastern Brazilian coastline. Quat. Sci. Rev. 25, 486–506. https://doi.org/10.1016/j.quascirev.2005.03.008

Angulo, R.J., Giannini, P.C.F., Souza, M.C. De, Lessa, G.C., Angulo, R.J., Giannini, P.C.F., Souza, M.C. De, Lessa, G.C., 2016. Holocene paleo-sea level changes along the coast of Rio de Janeiro, southern Brazil: Comment on Castro et al. (2014). An. Acad. Bras. Cienc. 88, 2105–2111. https://doi.org/10.1590/0001-3765201620140641

Aragón-Moreno, A.A., Islebe, G.A., Torrescano-Valle, N., Arellano-Verdejo, J., 2018.

Middle and late Holocene mangrove dynamics of the Yucatan Peninsula, Mexico. J. South Am. Earth Sci. 85, 307–311. https://doi.org/10.1016/j.jsames.2018.05.015

Beebower, J.R., 1964. Cyclothems and cyclic depositional mechanism in alluvial plain sedimentation. Bull. Kans. Univ. Geol. Surv. 169, 35–42.

Behling, H., Cohen, M.C.L., Lara, R.J., 2001. Studies on Holocene mangrove ecosystem dynamics of the Bragança Peninsula in north-eastern Pará, Brazil. Bosque 167, 225–242.

Behling, H., Cohen, M.L., Lara, R., 2004. Late Holocene mangrove dynamics of Marajó Island in Amazonia, northern Brazil. Veg. Hist. Archaeobot. 13, 73–80. https://doi.org/10.1007/s00334-004-0031-1

Benson, A., 2010. Rangia cuneata. USGS Nonindigenous Aquatic Species Database, Gainesville,FL. [online] Available from https://www.fws.gov/fisheries/ans/erss/uncertainrisk/Rangia-cuneata-WEB-10-01-12.pdf (Accessed 12 April 2020).

Blasco, F., 1996. Mangroves as indicators of coastal change. Catena 27, 167–178.

Blasco, F., Saenger, P., Janodet, E., 1996. Mangroves as indicators of coastal change. CATENA 27, 167–178. https://doi.org/10.1016/0341-8162(96)00013-6

Blum, M.D., Carter, A.E., Zayac, T., Goble, R., 2002. Middle Holocene Sea-Level and Evolution of The Gulf of Mexico Coast (USA). J. Coast. Res. 36, 65–80. https://doi.org/10.2112/1551-5036-36.sp1.65

Blum, M.D., Roberts, H.H., 2012. The Mississippi Delta Region: Past, Present, and Future. Annu. Rev. Earth Planet. Sci. 40, 655–683. https://doi.org/10.1146/annurev-earth-042711-105248

Braconnot, P., Otto-Bliesner, B., Harrison, S., Joussaume, S., Peterchmitt, J.Y., Abe-Ouchi, A., Crucifix, M., Driesschaert, E., Fichefet, T., Hewitt, C.D., Kageyama, M., Kitoh, A., Laîné, A., Loutre, M.F., Marti, O., Merkel, U., Ramstein, G., Valdes, P., Weber, S.L., Yu, Y., Zhao, Y., 2007. Results of PMIP2 coupled simulations of the Mid-Holocene and last glacial maximum - Part 1: Experiments and large-scale features. Clim. Past 3, 261–277. https://doi.org/10.5194/cp-3-261-2007

Bradley, R.S., Jones, P.D., 1992. When was the “Little Ice Age”?, in: Mikami, T. (Ed.), Proceedings of the International Symposium on the “Little Ice Age” Climate, Department of Geography, Tokyo Metropolitan University. pp. 1–4.

Brantley, S.T., Bissett, S.N., Young, D.R., Wolner, C.W. V., Moore, L.J., 2014. Barrier Island Morphology and Sediment Characteristics Affect the Recovery of Dune Building Grasses following Storm-Induced Overwash. PLoS One 9, e104747. https://doi.org/10.1371/journal.pone.0104747

Broecker, W.S., Stocker, T.F., 2006. The Holocene CO2 rise: Anthropogenic or natural? Eos (Washington. DC). 87, 27. https://doi.org/10.1029/2006EO030002

Brush, G.S., Brush, L.M., 1972. Transport of pollen in a sediment-laden channel; a laboratory study. Am. J. Sci. 272, 359–381. https://doi.org/10.2475/ajs.272.4.359

Buso Junior, A.A., Pessenda, L.C.R., Oliveira, P.E., Giannini, P.C., Cohen, M.C.L., Volkmer-Ribeiro, C., Barros de Oliveira, S.M., Favaro, D.I.T., Rossetti, D.F., Lorente, F., Borotti Filho, M.A., Schiavo, J.A., Bendassolli, J.A., França, M.C.,

Guimaraes, J.F.., Siqueira, G.., 2013. From an Estuary to a Freshwater Lake: A Paleo-Estuary Evolution in the Context of Holocene Sea-Level Fluctuations, Southeastern Brazil. Radiocarbon 55, 1735–1746. https://doi.org/10.2458/azu_js_rc.55.16210

Caballero, M., Peinalba, M.C., Martinez, M., Ortega-Guerrerol, B., Vazquez, L., 2005. A Holocene record from a former coastal lagoon in Bahia Kino, Gulf of California, Mexico. The Holocene 15, 1236–1244. https://doi.org/10.1191/0959683605hl896rr

Caldas, L.H. de O., Oliveira, J.G. de M., Stattegger, W.E. de, Stattegger, K., Vital, H., 2006. Geometry and evolution of Holocene transgressive and regressive barriers on the semi-arid coast of NE Brazil. Geo-Marine Lett. 26, 249–263. https://doi.org/10.1007/s00367-006-0034-2

Cannon, C.H., Morley, R.J., Bush, A.B.G., 2009. The current refugial rainforests of Sundaland are unrepresentative of their biogeographic past and highly vulnerable to disturbance. Proc. Natl. Acad. Sci. U. S. A. 106, 11188–11193. https://doi.org/10.1073/pnas.0809865106

Cavanaugh, K.C., Dangremond, E.M., Doughty, C.L., Park Williams, A., Parker, J.D., Hayes, M.A., Rodriguez, W., Feller, I.C., 2019. Climate-driven regime shifts in a mangrove–salt marsh ecotone over the past 250 years. Proc. Natl. Acad. Sci. U. S. A. 116, 21602–21608. https://doi.org/10.1073/pnas.1902181116

Cavanaugh, K. C., Kellner, J.R., Forde, A.J., Gruner, D.S., Parker, J.D., Rodriguez, W., Feller, I.C., 2014. Poleward expansion of mangroves is a threshold response to decreased frequency of extreme cold events. Proc. Natl. Acad. Sci. 111, 723–727. https://doi.org/10.1073/pnas.1315800111

Cavanaugh, Kyle C., Kellner, J.R., Forde, A.J., Gruner, D.S., Parker, J.D., Rodriguez, W., Feller, I.C., 2014. Poleward expansion of mangroves is a threshold response to decreased frequency of extreme cold events. Proc. Natl. Acad. Sci. U. S. A. 111, 723–727. https://doi.org/10.1073/pnas.1315800111

Cavanaugh, K.C., Osland, M.J., Bardou, R., Hinojosa-Arango, G., López-Vivas, J.M., Parker, J.D., Rovai, A.S., 2018. Sensitivity of mangrove range limits to climate variability. Glob. Ecol. Biogeogr. 27, 925–935. https://doi.org/10.1111/geb.12751

Cavanaugh, K.C., Parker, J.D., Cook-Patton, S.C., Feller, I.C., Williams, A.P., Kellner, J.R., 2015. Integrating physiological threshold experiments with climate modeling to project mangrove species' range expansion. Glob. Chang. Biol. 21, 1928–1938. https://doi.org/10.1111/gcb.12843

Cecil, C.B., 2013. An overview and interpretation of autocyclic and allocyclic processes and the accumulation of strata during the Pennsylvanian–Permian transition in the central Appalachian Basin, USA. Int. J. Coal Geol. 119, 21–31. https://doi.org/10.1016/j.coal.2013.07.012

Chapman, V.J., 1975. Mangrove biogeography, in: Walsh, G.E., Snedaker, S.C., Teas, H.J. (Eds.), International Symposium on Biology and Management of Mangroves. University of Florida Press, Miami, pp. 179–212.

Clark, P.U., Dyke, A.S., Shakun, J.D., Carlson, A.E., Clark, J., Wohlfarth, B., Mitrovica, J.X., Hostetler, S.W., McCabe, A.M., 2009. The Last Glacial Maximum. Science 325, 710–4. https://doi.org/10.1126/science.1172873

Cohen, M.C.L., Alves, I.C.C., França, M.C., Pessenda, L.C.R., Rossetti, D. de F., 2015.

790 Relative sea-level and climatic changes in the Amazon littoral during the last
791 500years. CATENA 133, 441–451. https://doi.org/10.1016/j.catena.2015.06.012

792 Cohen, M.C.L., Behling, H., Lara, R.J., 2005a. Amazonian mangrove dynamics during
793 the last millennium: The relative sea-level and the Little Ice Age. Rev. Palaeobot.
794 Palynol. 136, 93–108. https://doi.org/10.1016/j.revpalbo.2005.05.002

795 Cohen, M.C.L., Behling, H., Lara, R.J., Smith, C.B., Matos, H.R.S., Vedel, V., 2009.
796 Impact of sea-level and climatic changes on the Amazon coastal wetlands during
797 the late Holocene. Veg. Hist. Archaeobot. 18, 425–439.
798 https://doi.org/10.1007/s00334-008-0208-0

799 Cohen, M.C.L., Figueiredo, B.L., Oliveira, N.N., Fontes, N.A., França, M.C., Pessenda,
800 L.C.R., de Souza, A. V., Macario, K., Giannini, P.C.F., Bendassolli, J.A., Lima, P.,
801 2020a. Impacts of Holocene and modern sea-level changes on estuarine mangroves
802 from northeastern Brazil. Earth Surf. Process. Landforms 45, 375–392.
803 https://doi.org/10.1002/esp.4737

804 Cohen, M.C.L., França, M.C., Rossetti, D., Pessenda, L.C.R., Giannini, P.C.F., Lorente,
805 F.L., Junior, A.Á.B., Castro, D., Macario, K., 2014. Landscape evolution during
806 the late Quaternary at the Doce River mouth, Espírito Santo State, Southeastern
807 Brazil. Palaeogeogr. Palaeoclimatol. Palaeoecol. 415, 48–58.
808 https://doi.org/10.1016/j.palaeo.2013.12.001

809 Cohen, M.C.L., Lara, R.J., Cuevas, E., Oliveras, E.M., Da Silveira Sternberg, L., 2016.
810 Effects of sea-level rise and climatic changes on mangroves from southwestern
811 littoral of Puerto Rico during the middle and late Holocene. Catena 143.
812 https://doi.org/10.1016/j.catena.2016.03.041

813 Cohen, M.C.L., Lara, R.J., Smith, C.B., Angélica, R.S., Dias, B.S., Pequeno, T., 2008.
814 Wetland dynamics of Marajó Island, northern Brazil, during the last 1000 years.
815 CATENA 76, 70–77.

816 Cohen, M.C.L., Pessenda, L.C.R., Behling, H., de Fátima Rossetti, D., França, M.C.,
817 Guimarães, J.T.F., Friaes, Y., Smith, C.B., 2012. Holocene palaeoenvironmental
818 history of the Amazonian mangrove belt. Quat. Sci. Rev. 55, 50–58.

819 Cohen, M.C.L., Pessenda, L.C.R., Smith, C.B., GUIMARÃES, J.T.F., FRANÇA, M.C.,
820 2014. Amazonian Mangroves During the Late Pleistocene and Holocene, in:
821 Carvalho, I. de S., Garcia, M., Lana, C.C., Strohschoen, O. (Eds.), Paleontologia:
822 Cenários de Vida - Paleoclimas. Interciência, Rio de Janeiro, pp. 387–402.

823 Cohen, M.C.L., Rodrigues, E., Rocha, D.O.S., Freitas, J., Fontes, N.A., Pessenda,
824 L.C.R., de Souza, A. V., Gomes, V.L.P., França, M.C., Bonotto, D.M.,
825 Bendassolli, J.A., 2020b. Southward migration of the austral limit of mangroves in
826 South America. CATENA 195, 104775.
827 https://doi.org/10.1016/j.catena.2020.104775

828 Cohen, M. C.L., Rossetti, D.F., Pessenda, L.C.R., Friaes, Y.S., Oliveira, P.E., 2014.
829 Late Pleistocene glacial forest of Humaitá-Western Amazonia. Palaeogeogr.
830 Palaeoclimatol. Palaeoecol. 415, 37–47.
831 https://doi.org/10.1016/j.palaeo.2013.12.025

832 Cohen, M.C.L., Souza Filho, P.W.M., Lara, R.J., Behling, H., Angulo, R.J., 2005b. A
833 model of Holocene mangrove development and relative sea-level changes on the
834 Bragança Peninsula (northern Brazil). Wetl. Ecol. Manag. 13, 433–443.

https://doi.org/10.1007/s11273-004-0413-2

Cordero-Oviedo, C., Correa-Metrio, A., Urrego, L.E., Vázquez, G., Blaauw, M., Escobar, J., Curtis, J.H., 2019. Holocene establishment of mangrove forests in the western coast of the Gulf of Mexico. Catena 180, 212–223. https://doi.org/10.1016/j.catena.2019.04.025

Cuven, S., Paris, R., Falvard, S., Miot-Noirault, E., Benbakkar, M., Schneider, J.L., Billy, I., 2013. High-resolution analysis of a tsunami deposit: Case-study from the 1755 lisbon tsunami in southwestern spain. Mar. Geol. 337, 98–111. https://doi.org/10.1016/j.margeo.2013.02.002

Davis, M.B., 2000. Palynology after Y2K — Understanding the source area of pollen in sediments. Annu. Rev. Earth Planet. Sci 28, 1–18.

Deines, P., 1980. The isotopic composition of reduced organic carbon, in: Fritz, P., Fontes, J.C. (Eds.), Handbook of Environmental Isotope Geochemistry. The Terrestrial Environments. Elsevier, Amsterdam, pp. 329–406.

Deines, Peter, 1980. the Isotopic Composition of Reduced Organic Carbon. Terr. Environ. A. https://doi.org/10.1016/B978-0-444-41780-0.50015-8

Dietz, M., Liu, K., Bianchette, T., Dietz, M.E., Liu, K., Bianchette, T.A., 2018. Hurricanes as a Major Driver of Coastal Erosion in the Mississippi River Delta: A Multi-Decadal Analysis of Shoreline Retreat Rates at Bay Champagne, Louisiana (USA). Water 10, 1480. https://doi.org/10.3390/w10101480

Dittmar, T., Hertkorn, N., Kattner, G., Lara, R.J., 2006. Mangroves, a major source of dissolved organic carbon to the oceans. Global Biogeochem. Cycles 20, n/a-n/a. https://doi.org/10.1029/2005GB002570

Donnelly, C., Kraus, N., Larson, M., 2006. State of knowledge on measurement and modeling of coastal overwash. J. Coast. Res. 22, 965–991. https://doi.org/10.2112/04-0431.1

Donoghue, J.F., 2011. Sea level history of the northern Gulf of Mexico coast and sea level rise scenarios for the near future. Clim. Change 107, 17–33. https://doi.org/10.1007/s10584-011-0077-x

Duke, N.C., 1992. Mangrove floristics and biogeography. American Geophysical Union (AGU), pp. 63–100. https://doi.org/10.1029/CE041p0063

Duke, N.C., Ball, M.C., Ellison, J.C., 1998. Factors influencing biodiversity and distributional gradients in mangroves. Glob. Ecol. Biogeogr. Lett. 7, 27–47. https://doi.org/10.2307/2997695

Everitt, J.H., Judd, F.W., Escobar, D.E., Davis, M.R., 1996. Integration of remote sensing and spatial information technologies for mapping black mangrove on the Texas gulf coast. J. Coast. Res. 12, 64–69.

Ewel, K.C., Twilley, R.R., Ong, J.E., 1998. Different kinds of mangrove forests provide different goods and services. Glob. Ecol. Biogeogr. Lett. 7, 83–94.

Finkelstein, S.A., 2003. Identifying pollen grains of Typha latifolia, Typha angustifolia, and Typha xglauca. Can. J. Bot. 81, 985–990. https://doi.org/10.1139/b03-084

Fisher, R., Huo, J., 2012. A Business Plan for Blue Carbon Offsets at Duke University. Master of Environmental Management degree in the Nicholas School of the Environment of Duke University. .

Fontes, N.A., Moraes, C.A., Cohen, M.C.L., Alves, I.C.C., França, M.C., Pessenda, L.C.R., Francisquini, M.I., Bendassolli, J.A., Macario, K., Mayle, F., 2017. The Impacts of the Middle Holocene High Sea-Level Stand and Climatic Changes on Mangroves of the Jucuruçu River, Southern Bahia – Northeastern Brazil. Radiocarbon 59, 215–230. https://doi.org/10.1017/RDC.2017.6

Food and Agriculture Organization of the United Nations., 2007. The world's mangroves, 1980-2005 : a thematic study in the framework of the Global Forest Resources Assessment 2005. Food and Agriculture Organization of the United Nations.

França, M.C., Alves, I.C.C., Castro, D.F., Cohen, M.C.L., Rossetti, D.F., Pessenda, L.C.R., Lorente, F.L., Fontes, N.A., Junior, A.Á.B., Giannini, P.C.F., Francisquini, M.I., 2015. A multi-proxy evidence for the transition from estuarine mangroves to deltaic freshwater marshes, Southeastern Brazil, due to climatic and sea-level changes during the late Holocene. CATENA 128, 155–166. https://doi.org/10.1016/j.catena.2015.02.005

Franca, M.C., Alves, I.C.C., Cohen, M.C., Rossetti, D.F., Pessenda, L.C., Giannini, P.C., Lorente, F.L., Buso Junior, A.A., Bendassolli, J.A., Macario, K., 2016. Millennial to secular time-scale impacts of climate and sea-level changes on mangroves from the Doce River delta, Southeastern Brazil. The Holocene 26, 1733–1749. https://doi.org/10.1177/0959683616645938

França, M.C., Cohen, M.C.L., Pessenda, L.C.R., Rossetti, D.F., Lorente, F.L., Buso Junior, A.Á., Guimarães, J.T.F., Friaes, Y., Macario, K., 2013. Mangrove vegetation changes on Holocene terraces of the Doce River, southeastern Brazil. CATENA 110, 59–69.

França, M.C., Francisquini, M.I., Cohen, M.C.L., Pessenda, L.C.R., 2014. Inter-proxy evidence for the development of the Amazonian mangroves during the Holocene. Veg. Hist. Archaeobot. 23, 527–542. https://doi.org/10.1007/s00334-013-0420-4

França, M.C., Pessenda, L.C., Cohen, M.C., de Azevedo, A.Q., Fontes, N.A., Silva, F.B., de Melo, J.C., Piccolo, M. de C., Bendassolli, J.A., Macario, K., 2019. Late-Holocene subtropical mangrove dynamics in response to climate change during the last millennium. The Holocene 29, 445–456. https://doi.org/10.1177/0959683618816438

Fromard, F., Vega, C., Proisy, C., 2004a. Half a century of dynamic coastal change affecting mangrove shorelines of French Guiana. A case study based on remote sensing data analyses and field surveys. Mar. Geol. 208, 265–280. https://doi.org/10.1016/j.margeo.2004.04.018

Fromard, F., Vega, C., Proisy, C., 2004b. Half a century of dynamic coastal change affecting mangrove shorelines of French Guiana. A case study based on remote sensing data analyses and field surveys. Mar. Geol. 208, 265–280. https://doi.org/10.1016/j.margeo.2004.04.018

Giri, C., Ochieng, E., Tieszen, L.L., Zhu, Z., Singh, A., Loveland, T., Masek, J., Duke, N., 2011. Status and distribution of mangrove forests of the world using earth observation satellite data. Glob. Ecol. Biogeogr. 20, 154–159. https://doi.org/10.1111/j.1466-8238.2010.00584.x

Gischler, E., 2015. Quaternary reef response to sea-level and environmental change in the western Atlantic. Sedimentology 62, 429–465.

925 https://doi.org/10.1111/sed.12174

926 Gosling, W.D., Mayle, F.E., Tate, N.J., Killeen, T.J., 2009. Differentiation between
927 Neotropical rainforest, dry forest, and savannah ecosystems by their modern pollen
928 spectra and implications for the fossil pollen record. Rev. Palaeobot. Palynol. 153,
929 70–85. https://doi.org/10.1016/j.revpalbo.2008.06.007

930 Grimm, E., 1990. TILIA and TILIAGRAPH: PC spreadsheet and graphic software for
931 pollen data, INQUA Sub-Commission on Data-Handling Methods Newsletter.

932 Guimarães, J.T.F., Cohen, M.C.L., Franca, M.C., Pessenda, L.C.R., Behling, H., 2013.
933 Morphological and vegetation changes on tidal flats of the Amazon Coast during
934 the last 5000 cal. yr BP. The Holocene 23, 528–543.
935 https://doi.org/10.1177/0959683612463097

936 Guimarães, J.T.F., Cohen, M.C.L., Pessenda, L.C.R., Franca, M.C., Smith, C.B.,
937 Nogueira, a. C.R., 2011. Mid- and late-Holocene sedimentary process and
938 palaeovegetation changes near the mouth of the Amazon River. The Holocene 22,
939 359–370. https://doi.org/10.1177/0959683611423693

940 Hamdi, S.M.M., Assadi, M., Segarra-Moragues, J.G., 2010. Pollen morphology of
941 Iranian species of Typha L. (Typhaceae) and its taxonomic significance. Feddes
942 Repert. 121, 85–96. https://doi.org/10.1002/fedr.200911130

943 Hameed, M., Nawaz, T., Ashraf, M., Tufail, A., Kanwal, H., Sajid Aqeel Ahmad, M.,
944 Ahmad, I., 2012. LEAF ANATOMICAL ADAPTATIONS OF SOME
945 HALOPHYTIC AND XEROPHYTIC SEDGES OF THE PUNJAB.

946 Harper, C., 1984. Improved methods of facies sequence analysis. Facies Model.

947 Harris, M.S., Sautter, L.R., Johnson, K.L., Luciano, K.E., Sedberry, G.R., Wright, E.E.,
948 Siuda, A.N.S., 2013. Continental shelf landscapes of the southeastern United States
949 since the last interglacial. Geomorphology 203, 6–24.
950 https://doi.org/10.1016/j.geomorph.2013.02.014

951 Havinga, A.J., 1967. Palynology and pollen preservation. Rev. Paleobotany Palynol. 2,
952 81–98.

953 Henry, K.M., Twilley, R.R., 2013. Soil Development in a Coastal Louisiana Wetland
954 during a Climate-Induced Vegetation Shift from Salt Marsh to Mangrove. J. Coast.
955 Res. 292, 1273–1283. https://doi.org/10.2112/JCOASTRES-D-12-00184.1

956 Jafari, N.H., Harris, B.D., Stark, T.D., 2018. Geotechnical investigations at the
957 caminada headlands beach and dune in coastal Louisiana. Coast. Eng. 142, 82–94.
958 https://doi.org/10.1016/j.coastaleng.2018.04.014

959 Joe-Wong, C., Schlesinger, D.R., Chow, A.T., Myneni, S.C.B., 2019. Sea level rise
960 produces abundant organobromines in salt-affected coastal wetlands. Geochem.
961 Persp. Let 10, 31–35. https://doi.org/10.7185/geochemlet.1911

962 Johnson, C.L., Chen, Q., Ozdemir, C.E., 2020. Lidar time-series analysis of a rapidly
963 transgressing low-lying mainland barrier (Caminada Headlands, Louisiana, USA).
964 Geomorphology 352, 106979. https://doi.org/10.1016/j.geomorph.2019.106979

965 Jomelli, V., Khodri, M., Favier, V., Brunstein, D., Ledru, M.-P., Wagnon, P., Blard, P.-
966 H., Sicart, J.-E., Braucher, R., Grancher, D., Bourlè, L., Braconnot, P., Vuille, M.,
967 2011. Irregular tropical glacier retreat over the Holocene epoch driven
968 by92nprogressive warming. Nature. https://doi.org/10.1038/nature10150

969 Jones, M.C., Wingard, G.L., Stackhouse, B., Keller, K., Willard, D., Marot, M.,
970 Landacre, B., E. Bernhardt, C., 2019. Rapid inundation of southern Florida
971 coastline despite low relative sea-level rise rates during the late-Holocene. Nat.
972 Commun. 10, 1–13. https://doi.org/10.1038/s41467-019-11138-4

973 Kaplan, J.O., Krumhardt, K.M., Ellis, E.C., Ruddiman, W.F., Lemmen, C., Goldewijk,
974 K.K., 2011. Holocene carbon emissions as a result of anthropogenic land cover
975 change. Holocene 21, 775–791. https://doi.org/10.1177/0959683610386983

976 Kennedy, J.P., Pil, M.W., Proffitt, C.E., Boeger, W.A., Stanford, A.M., Devlin, D.J.,
977 2016. Postglacial expansion pathways of red mangrove, Rhizophora mangle, in the
978 Caribbean Basin and Florida. Am. J. Bot. 103, 260–276.
979 https://doi.org/10.3732/ajb.1500183

980 Khan, N.S., Ashe, E., Horton, B.P., Dutton, A., Kopp, R.E., Brocard, G., Engelhart,
981 S.E., Hill, D.F., Peltier, W.R., Vane, C.H., Scatena, F.N., 2017. Drivers of
982 Holocene sea-level change in the Caribbean. Quat. Sci. Rev.
983 https://doi.org/10.1016/j.quascirev.2016.08.032

984 Kjerfve, B., 1994. Coastal Lagoons. Elsevier Oceanogr. Ser. 60, 1–8.
985 https://doi.org/10.1016/S0422-9894(08)70006-0

986 Krauss, K.W., Lovelock, C.E., McKee, K.L., López-Hoffman, L., Ewe, S.M.L., Sousa,
987 W.P., 2008. Environmental drivers in mangrove establishment and early
988 development: A review. Aquat. Bot. 89, 105–127.
989 https://doi.org/10.1016/j.aquabot.2007.12.014

990 Krauss, K.W., McKee, K.L., Lovelock, C.E., Cahoon, D.R., Saintilan, N., Reef, R.,
991 Chen, L., 2014. How mangrove forests adjust to rising sea level. New Phytol. 202,
992 19–34. https://doi.org/10.1111/nph.12605

993 Kulp, M., Penland, S., Williams, S.J., Jenkins, C., Flocks, J., Kindinger, J., 2005.
994 Geologic Framework, Evolution, and Sediment Resources for Restoration of the
995 Louisiana Coastal Zone. J. Coast. Res. https://doi.org/10.2307/25737049

996 Ladislas, S., El-Mufleh, A., Gérente, C., Chazarenc, F., Andrès, Y., Béchet, B., 2012.
997 Potential of aquatic macrophytes as bioindicators of heavy metal pollution in urban
998 stormwater runoff. Water. Air. Soil Pollut. 223, 877–888.
999 https://doi.org/10.1007/s11270-011-0909-3

1000 Lara, R.J., Cohen, M.C.L., 2009. Palaeolimnological studies and ancient maps confirm
1001 secular climate fluctuations in Amazonia. Clim. Change 94, 399–408.
1002 https://doi.org/10.1007/s10584-008-9507-9

1003 Lara, R.J., Cohen, M.C.L., 2006. Sediment porewater salinity, inundation frequency and
1004 mangrove vegetation height in Bragança, North Brazil: an ecohydrology-based
1005 empirical model. Wetl. Ecol. Manag. 14, 349–358. https://doi.org/10.1007/s11273-
1006 005-4991-4

1007 Lean, J., Rind, D., 1999. Evaluating sun-climate relationships since the Little Ice Ag.
1008 Jounal Amospheric Solar-Terrestrial Phys. 61, 25–36.

1009 Lima, W.J.S., Cohen, M.C.L., Rossetti, D.F., França, M.C., 2017. Late Pleistocene
1010 glacial forest elements of Brazilian Amazonia. Palaeogeogr. Palaeoclimatol.
1011 Palaeoecol. https://doi.org/10.1016/j.palaeo.2017.11.050

1012 Liu, K., 2004. Paleotempestology: Principles, methods, and examples from Gulf coast
1013 lake-sediments, in: Murnane, R., Liu, K.B. (Eds.), Hurricanes and Typhoons: Past,

Present, and Future. Columbia University, New York, pp. 13–57.

Liu, K., Li, C., Bianchette, T., McCloskey, T., 2011. Storm Deposition in a Coastal Backbarrier Lake in Louisiana Caused by Hurricanes Gustav and Ike. J. Coast. Res. 64, 1866–1870.

Liu, K.B., McCloskey, T.A., Bianchette, T.A., Keller, G., Lam, N.S.N., Cable, J.E., Arriola, J., 2015. Hurricane Isaac storm surge deposition in a coastal wetland along Lake Pontchartrain, southern Louisiana. J. Coast. Res. 70, 266–271. https://doi.org/10.2112/SI70-045.1

Liu, Z., Zhu, J., Rosenthal, Y., Zhang, X., Otto-Bliesner, B.L., Timmermann, A., Smith, R.S., Lohmann, G., Zheng, W., Timm, O.E., 2014. The Holocene temperature conundrum. Proc. Natl. Acad. Sci. U. S. A. 111, E3501–E3505. https://doi.org/10.1073/pnas.1407229111

Lloyd, F.E., Tracy, S.M., 1901. The Insular Flora of Mississippi and Louisiana. Bull. Torrey Bot. Club 28, 61. https://doi.org/10.2307/2477884

Lohmann, G., Pfeiffer, M., Laepple, T., Leduc, G., Kim, J.H., 2013. A model-data comparison of the Holocene global sea surface temperature evolution. Clim. Past 9, 1807–1839. https://doi.org/10.5194/cp-9-1807-2013

Lorente, F.L., Pessenda, L.C.R., Oboh-Ikuenobe, F., Buso Jr., A.A., Cohen, M.C.L., Meyer, K.E.B., Giannini, P.C.F., de Oliveira, P.E., Rossetti, D. de F., Borotti Filho, M.A., França, M.C., de Castro, D.F., Bendassolli, J.A., Macario, K., 2013. Palynofacies and stable C and N isotopes of Holocene sediments from Lake Macuco (Linhares, Espírito Santo, southeastern Brazil): Depositional settings and palaeonvironmental evolution. Palaeogeogr. Palaeoclimatol. Palaeoecol. 55, 325–330. https://doi.org/10.1016/j.palaeo.2013.12.004

Lugo, A.E., Patterson-zucca, C., 1977. The impact of low temperature stress on mangrove structure and growth.

McKee, K.L., Vervaeke, W.C., 2018. Will fluctuations in salt marsh–mangrove dominance alter vulnerability of a subtropical wetland to sea-level rise? Glob. Chang. Biol. 24, 1224–1238. https://doi.org/10.1111/gcb.13945

McLeod, E., Salm, R.V., 2006. Managing Mangroves for Resilience to Climate Change. IUCN, Gland, Switzerland.

Meyer, H., Opel, T., Laepple, T., Dereviagin, A.Y., Hoffmann, K., Werner, M., 2015. Long-term winter warming trend in the Siberian Arctic during the mid- to late Holocene. Nat. Geosci. 8, 122–125. https://doi.org/10.1038/ngeo2349

Meyers, Philip A., 1994. Preservation of elemental and isotopic source identification of sedimentary organic matter. Chem. Geol. 114, 289–302. https://doi.org/10.1016/0009-2541(94)90059-0

Meyers, P.A., 1994. Preservation of elemental and isotopic source identification of sedimentary organic matter. Chem. Geol. 114, 289–302.

Miall, A.D., 1978. Lithofacies types and vertical profile models in braided river deposits: a summary. Fluv. Sedimentol. 5, 597–600.

Mock, C.J., Mojzisek, J., McWaters, M., Chenoweth, M., Stahle, D.W., 2007. The winter of 1827-1828 over eastern North America: A season of extraordinary climatic anomalies, societal impacts, and false spring. Clim. Change 83, 87–115.

https://doi.org/10.1007/s10584-006-9126-2

Montoya, E., Pedra-Méndez, J., García-Falcó, E., Gómez-Paccard, M., Giralt, S., Vegas-Vilarrúbia, T., Stauffer, F.W., Rull, V., 2019. Long-term vegetation dynamics of a tropical megadelta: Mid-Holocene palaeoecology of the Orinoco Delta (NE Venezuela). Quat. Sci. Rev. https://doi.org/10.1016/j.quascirev.2019.105874

Moraes, C.A., Fontes, N.A., Cohen, M.C., França, M.C., Pessenda, L.C., Rossetti, D.F., Francisquini, M.I., Bendassolli, J.A., Macario, K., 2017. Late Holocene mangrove dynamics dominated by autogenic processes. Earth Surf. Process. Landforms. https://doi.org/10.1002/esp.4167

Moraes, Caio A., Fontes, N.A., Cohen, M.C.L., França, M.C., Pessenda, L.C.R., Rossetti, D.F., Francisquini, M.I., Bendassolli, J.A., Macario, K., 2017. Late Holocene mangrove dynamics dominated by autogenic processes. Earth Surf. Process. Landforms. https://doi.org/10.1002/esp.4167

Mulvaney, R., Abram, N.J., Hindmarsh, R.C.A., Arrowsmith, C., Fleet, L., Triest, J., Sime, L.C., Alemany, O., Foord, S., 2012. Recent Antarctic Peninsula warming relative to Holocene climate and ice-shelf history. Nature 489, 141–144. https://doi.org/10.1038/nature11391

Murray-Wallace, C.V., 2007. Eustatic sea-level changes since the last glaciation, in: ELIAS, S.A. (Ed.), Encyclopedia of Quaternary Science. Elsevier, Amsterdam, pp. 3034–3043.

Naquin, J.D., Liu, K., McCloskey, T.A., Bianchette, T.A., 2014a. Storm deposition induced by hurricanes in a rapidly subsiding coastal zone. J. Coast. Res. 70, 308–313. https://doi.org/10.2112/si70-052.1

Naquin, J.D., Liu, K., McCloskey, T.A., Bianchette, T.A., 2014b. Storm deposition induced by hurricanes in a rapidly subsiding coastal zone. J. Coast. Res. 70, 308–313. https://doi.org/10.2112/SI70-052.1

Nielsen, S.H.H., Koç, N., Crosta, X., 2004. Holocene climate in the Atlantic sector of the Southern Ocean: Controlled by insolation or oceanic circulation? Geology 32, 317–320. https://doi.org/10.1130/G20334.1

Nittrouer, C.A., Kuehl, S.A., Figueiredo, G., Allison, M.A., K, I.I.C., Rine, J.M., Faria, T.L.E.C., Silveira, O.M., 1996. The geological record preserved by Amazon shelf sedimentation 16.

O'ishi, R., Abe-Ouchi, A., 2011. Polar amplification in the mid-Holocene derived from dynamical vegetation change with a GCM. Geophys. Res. Lett. 38, n/a-n/a. https://doi.org/10.1029/2011GL048001

Osland, M.J., Day, R.H., From, A.S., McCoy, M.L., McLeod, J.L., Kelleway, J.J., 2015. Life stage influences the resistance and resilience of black mangrove forests to winter climate extremes. Ecosphere 6, art160. https://doi.org/10.1890/ES15-00042.1

Osland, M.J., Day, R.H., Hall, C.T., Brumfield, M.D., Dugas, J.L., Jones, W.R., 2017. Mangrove expansion and contraction at a poleward range limit: climate extremes and land-ocean temperature gradients. Ecology 98, 125–137. https://doi.org/10.1002/ecy.1625

Osland, M.J., Feher, L.C., 2020. Winter climate change and the poleward range

expansion of a tropical invasive tree (Brazilian pepper—Schinus terebinthifolius). Glob. Chang. Biol. 26, 607–615. https://doi.org/10.1111/gcb.14842

Osland, M.J., Feher, L.C., López-Portillo, J., Day, R.H., Suman, D.O., Guzmán Menéndez, J.M., Rivera-Monroy, V.H., 2018. Mangrove forests in a rapidly changing world: Global change impacts and conservation opportunities along the Gulf of Mexico coast. Estuar. Coast. Shelf Sci. 214, 120–140. https://doi.org/10.1016/j.ecss.2018.09.006

Osland, M.J., Hartmann, A.M., Day, R.H., Ross, M.S., Hall, C.T., Feher, L.C., Vervaeke, W.C., 2019. Microclimate Influences Mangrove Freeze Damage: Implications for Range Expansion in Response to Changing Macroclimate. Estuaries and Coasts 42, 1084–1096. https://doi.org/10.1007/s12237-019-00533-1

Peros, M.C., Reinhardt, E.G., Davis, A.M., 2007. A 6000-year record of ecological and hydrological changes from Laguna de la Leche, north coastal Cuba. Quat. Res. 67, 69–82. https://doi.org/10.1016/j.yqres.2006.08.004

Perry, C.L., Mendelssohn, I.A., 2009a. Ecosystem effects of expanding populations of Avicennia germinans in a Louisiana salt marsh. Wetlands 29, 396–406. https://doi.org/10.1672/08-100.1

Perry, C.L., Mendelssohn, I.A., 2009b. Ecosystem effects of expanding populations of Avicennia germinans in a Louisiana salt marsh. Wetlands 29, 396–406. https://doi.org/10.1672/08-100.1

Pessenda, L.C.R., Gouveia, S.E.M., Ribeiro, A. de S., De Oliveira, P.E., Aravena, R., 2010. Late Pleistocene and Holocene vegetation changes in northeastern Brazil determined from carbon isotopes and charcoal records in soils. Palaeogeogr. Palaeoclimatol. Palaeoecol. 297, 597–608. https://doi.org/10.1016/j.palaeo.2010.09.008

Pessenda, L.C.R., Ribeiro, A.D.S., Gouveia, S.E.M., Aravena, R., Boulet, R., Bendassolli, J.A., 2004. Vegetation dynamics during the late Pleistocene in the Barreirinhas region, Maranhão State, northeastern Brazil, based on carbon isotopes in soil organic matter. Quat. Res. 62, 183–193. https://doi.org/10.1016/j.yqres.2004.06.003

Pessenda, L.C.R., Vidotto, E., De Oliveira, P.E., Buso, A.A., Cohen, M.C.L., Rossetti, D. de F., Ricardi-Branco, F., Bendassolli, J.A., 2012. Late Quaternary vegetation and coastal environmental changes at Ilha do Cardoso mangrove, southeastern Brazil. Palaeogeogr. Palaeoclimatol. Palaeoecol. 363, 57–68.

Quisthoudt, K., Schmitz, N., Randin, C.F., Dahdouh-Guebas, F., Robert, E.M.R., Koedam, N., 2012. Temperature variation among mangrove latitudinal range limits worldwide. Trees - Struct. Funct. 26, 1919–1931. https://doi.org/10.1007/s00468-012-0760-1

Reading, H.G., 1996. Sedimentary Environments: Processes, Facies and Stratigraphy, 3a ed. Blackwell Science.

Reimer, P.J., Bard, E., Bayliss, A., Beck, J.W., Blackwell, P.G., Ramsey, C.B., Buck, C.E., Cheng, H., Edwards, R.L., Friedrich, M., Grootes, P.M., Guilderson, T.P., Haflidason, H., Hajdas, I., Hatté, C., Heaton, T.J., Hoffmann, D.L., Hogg, A.G., Hughen, K.A., Kaiser, K.F., Kromer, B., Manning, S.W., Niu, M., Reimer, R.W., Richards, D.A., Scott, E.M., Southon, J.R., Staff, R.A., Turney, C.S.M., van der

Plicht, J., 2013. IntCal13 and Marine13 Radiocarbon Age Calibration Curves 0–50,000 Years cal BP. Radiocarbon 55, 1869–1887. https://doi.org/10.2458/azu_js_rc.55.16947

Reineck, H.E., Singh, I.B., 1980. Depositional sedimentary environments, with reference to terrigenous clastics. Second edition (Textbook). Depos. Sediment. Environ. with Ref. to terrigenous clastics. Second Ed. (Textb.

Ribeiro, R. de A., Rovai, A.S., Twilley, R.R., Castañeda-Moya, E., 2019. Spatial variability of mangrove primary productivity in the neotropics. Ecosphere 10. https://doi.org/10.1002/ecs2.2841

Ribeiro, S.R., Batista, E.J.L., Cohen, M.C., França, M.C., Pessenda, L.C., Fontes, N.A., Alves, I.C., Bendassolli, J.A., 2018. Allogenic and autogenic effects on mangrove dynamics from the Ceará Mirim River, north-eastern Brazil, during the middle and late Holocene. Earth Surf. Process. Landforms. https://doi.org/10.1002/esp.4342

Rodriguez, A.B., Anderson, J.B., Siringan, F.P., Taviani, M., 2004. Holocene Evolution of the East Texas Coast and Inner Continental Shelf: Along-Strike Variability in Coastal Retreat Rates. J. Sediment. Res. 74, 405–421. https://doi.org/10.1306/092403740405

Rossetti, D.F., Cohen, M.C.L., Bertani, T.C., Hayakawa, E.H., Paz, J.D.S., Castro, D.F., Friaes, Y., 2014. Late Quaternary fluvial terrace evolution in the main southern Amazonian tributary. Catena 116. https://doi.org/10.1016/j.catena.2013.11.021

Roubik, D.W., Moreno, J.E., 1991. Pollen and Spores of Barro Colorado Island. Missouri Botanical Garden.

Ruddiman, W.F., 2003. The anthropogenic greenhouse era began thousands of years ago. Clim. Change. https://doi.org/10.1023/B:CLIM.0000004577.17928.fa

Ruddiman, W.F., Fuller, D.Q., Kutzbach, J.E., Tzedakis, P.C., Kaplan, J.O., Ellis, E.C., Vavrus, S.J., Roberts, C.N., Fyfe, R., He, F., Lemmen, C., Woodbridge, J., 2016. Late Holocene climate: Natural or anthropogenic? Rev. Geophys. https://doi.org/10.1002/2015RG000503

Ryu, J., 2020. Late Holocene Environmental Changes and Ecosystem Dynamics in Louisiana's Coastal Wetlands: A Multi-Site, Multi-Proxy Investigation. Louisiana State University.

Saintilan, N., Wilson, N.C., Rogers, K., Rajkaran, A., Krauss, K.W., 2014. Mangrove expansion and salt marsh decline at mangrove poleward limits. Glob. Chang. Biol. 20, 147–157. https://doi.org/10.1111/gcb.12341

Sandoval-Castro, E., Muñiz-Salazar, R., Enríquez-Paredes, L.M., Riosmena-Rodríguez, R., Dodd, R.S., Tovilla-Hernández, C., Arredondo-García, M.C., 2012a. Genetic population structure of red mangrove (Rhizophora mangle L.) along the northwestern coast of Mexico. Aquat. Bot. 99, 20–26. https://doi.org/10.1016/J.AQUABOT.2012.01.002

Sandoval-Castro, E., Muñiz-Salazar, R., Enríquez-Paredes, L.M., Riosmena-Rodríguez, R., Dodd, R.S., Tovilla-Hernández, C., Arredondo-García, M.C., 2012b. Genetic population structure of red mangrove (Rhizophora mangle L.) along the northwestern coast of Mexico. Aquat. Bot. 99, 20–26. https://doi.org/10.1016/J.AQUABOT.2012.01.002

Santos, T.P., Franco, D.R., Barbosa, C.F., Belem, A.L., Dokken, T., Albuquerque,

A.L.S., 2013. Millennial- to centennial-scale changes in sea surface temperature in the tropical South Atlantic throughout the Holocene. Palaeogeogr. Palaeoclimatol. Palaeoecol. 392, 1–8. https://doi.org/10.1016/j.palaeo.2013.08.019

Saucier, R.T., 1994. Geomorphology and Quaternary Geologic History of the Lower Mississippi Valley, Volume 1. ed. U. S. Army Corps of Engineers, Vicksburg.

Shea Penland, J.R.S., 1988. Barrier Island Erosion and Protection in Louisiana: A Coastal Geomorphological Perspective 38.

Sherrod, C.L., McMillan, C., 1985. The distributional history and ecology of mangrove vegetation along the northern Gulf of Mexico coastal region. Contrib Mar Sci 28, 129–140.

Silva, M.N.A., Cohen, M.C.L., Rossetti, D.F., Pessenda, L.C.R., 2018. Did Sea-Level Changes Affect the Brazilian Amazon Forest during the Holocene? Radiocarbon 60, 91–112. https://doi.org/10.1017/RDC.2017.62

Skvarla, J.J., Larson, D.A., 1963. Nature of cohesion within pollen tetrads of Typha latifolia. Science (80-.). 140, 173–175. https://doi.org/10.1126/science.140.3563.173

Smith, C.B., Cohen, M.C.L., Pessenda, L.C.R., França, M.C., Guimarães, J.T.F., 2012. Holocenic proxies of sedimentary organic matter and the evolution of Lake Arari-Amazon Region. CATENA 90, 26–38.

Smith, C.B., Cohen, M.C.L., Pessenda, L.C.R., França, M.C., Guimarães, J.T.F., Rossetti, D. de F., Lara, R.J., 2011. Holocene coastal vegetation changes at the mouth of the Amazon River. Rev. Palaeobot. Palynol. 168, 21–30.

Solomon, A.M., Blasing, T.J., Solomon, J.A., 1982. Interpretation of floodplain pollen in alluvial sediments from an Arid Region. Quat. Res. 18, 52–71.

Solomon, S., Qin, D., Manning, M., Chen, Z., Marquis, M., Averyl, K.B., Tignor, M., Miller, H.L., 2007. Climate Change 2007: The Physical Science Basis. Contribution of Working Group I to the Fourth Assessment Report of the Intergovernmental Panel on Climate Change, Cambridge University Press.

Stevens, P.W., Fox, S.L., Montague, C.L., 2006a. The interplay between mangroves and saltmarshes at the transition between temperate and subtropical climate in Florida. Wetl. Ecol. Manag. 14, 435–444. https://doi.org/10.1007/s11273-006-0006-3

Stevens, P.W., Fox, S.L., Montague, C.L., 2006b. The interplay between mangroves and saltmarshes at the transition between temperate and subtropical climate in Florida. Wetl. Ecol. Manag. 14, 435–444. https://doi.org/10.1007/s11273-006-0006-3

Stokes, D.J., Healy, T.R., Cooke, P.J., 2010. Expansion Dynamics of Monospecific, Temperate Mangroves and Sedimentation in Two Embayments of a Barrier-Enclosed Lagoon, Tauranga Harbour, New Zealand. J. Coast. Res. 261, 113–122. https://doi.org/10.2112/08-1043.1

Stuart, S A, Choat, B., Martin, K.C., Holbrook, N.M., Ball, M.C., 2007. The role of freezing in setting the latitudinal limits of mangrove forests. New Phytol. 173, 576–83. https://doi.org/10.1111/j.1469-8137.2006.01938.x

Stuart, S. A., Choat, B., Martin, K.C., Holbrook, N.M., Ball, M.C., 2007. The role of freezing in setting the latitudinal limits of mangrove forests. New Phytol. 173,

576–583. https://doi.org/10.1111/j.1469-8137.2006.01938.x

Sun, X., Li, X., 1999. A pollen record of the last 37 ka in deep sea core 17940 from the northern slope of the South China Sea. Mar. Geol. 156, 227–244. https://doi.org/10.1016/S0025-3227(98)00181-9

Sundqvist, H.S., Kaufman, D.S., McKay, N.P., Balascio, N.L., Briner, J.P., Cwynar, L.C., Sejrup, H.P., Seppä, H., Subetto, D.A., Andrews, J.T., Axford, Y., Bakke, J., Birks, H.J.B., Brooks, S.J., De Vernal, A., Jennings, A.E., Ljungqvist, F.C., Rühland, K.M., Saenger, C., Smol, J.P., Viau, A.E., 2014. Arctic Holocene proxy climate database – New approaches to assessing geochronological accuracy and encoding climate variables. Clim. Past 10, 1605–1631. https://doi.org/10.5194/cp-10-1605-2014

Taillardat, P., Friess, D.A., Lupascu, M., 2018. Mangrove blue carbon strategies for climate change mitigation are most effective at the national scale. Biol. Lett. 14, 20180251. https://doi.org/10.1098/rsbl.2018.0251

Timm, O., Timmermann, A., 2007. Simulation of the last 21 000 years using accelerated transient boundary conditions. J. Clim. 20, 4377–4401. https://doi.org/10.1175/JCLI4237.1

Tomlinsom, P.B., 1986. The Botany of Mangroves. Cambridge University Press, Cambridge.

Toscano, M.A., Macintyre, I.G., 2003. Corrected western Atlantic sea-level curve for the last 11,000 years based on calibrated 14C dates from Acropora palmata framework and intertidal mangrove peat. Coral Reefs 22, 257–270. https://doi.org/10.1007/s00338-003-0315-4

Tyson, R.V., 1995. Sedimentary Organic Matter: Organic Facies and Palynofacies. Chapman and Hall, London.

Vedel, V., Behling, H., Cohen, M., Lara, R., 2006. Holocene mangrove dynamics and sea-level changes in northern Brazil, inferences from the Taperebal core in northeastern Pará State. Veg. Hist. Archaeobot. 15, 115–123. https://doi.org/10.1007/s00334-005-0023-9

Vega, A.J., 2012. Louisiana Weather and Climate -Louisiana State University Baton Rouge [WWW Document]. URL https://books.google.com.br/books?id=0wglj5alm9oC&printsec=frontcover&hl=pt-BR#v=onepage&q&f=false (accessed 5.17.20).

Wakida-Kusunoki, A.T. MacKenzie, C.L., 2004. Rangia and marsh clams, Rangia cuneata, R. flexuosa, and Polymesoda caroliniana, in Eastern México: distribution, biology and ecology, and historical fisheries. Mar. Fish. Rev. 66, 13–20.

Walker, R.G., 1992. Facies, facies models and modern stratigrahic concepts, in: Walker, R.G., James, N.P. (Eds.), Facies Models - Response to Sea Level Change. Geological Association of Canada, Ontario, pp. 1–14.

Walsh, G.E., 1974. Mangroves: a review, in: Reinold, R.J., Queen, W.H. (Eds.), Ecology of Halophytes. Academic Press, New York, pp. 51-174.

Walsh, J.., Nittrouer, C.., 2004. Mangrove-bank sedimentation in a mesotidal environment with large sediment supply, Gulf of Papua. Mar. Geol. 208, 225–248. https://doi.org/10.1016/j.margeo.2004.04.010

Wanless, H.R., Parkinson, R.W., Tedesco, L.P., 1994. Sea level control on stability of Everglades wetlands., in: Davis, S.M., Ogden, J.C. (Eds.), Everglades: The Ecosystem and Its Restoration. St. Lucie Press, pp. 199–222.

Warzocha, J., Szymanek, L., Witalis, B., Wodzinowski, T., 2016. The first report on the establishment and spread of the alien clam Rangia cuneata (Mactridae) in the Polish part of the Vistula Lagoon (southern Baltic). Oceanologia 58, 54–58. https://doi.org/10.1016/j.oceano.2015.10.001

Weng, C., Bush, M.B., Silman, M.R., 2004. An analysis of modern pollen rain on an elevational gradient in southern Peru. J. Trop. Ecol. 20, 113–124. https://doi.org/10.1017/S0266467403001068

Willard, D.A., Bernhardt, C.E., 2011. Impacts of past climate and sea level change on Everglades wetlands: placing a century of anthropogenic change into a late-Holocene context. Clim. Change 107, 59–80. https://doi.org/10.1007/s10584-011-0078-9

Woodroffe, C.D., Grindrod, J., 1991. Mangrove Biogeography: The Role of Quaternary Environmental and Sea-Level Change. J. Biogeogr. 18, 479–492. https://doi.org/10.2307/2845685

Woodroffe, C.D., Thom, B.G., Chappell, J., 1985. Development of widespread mangrove swamps in mid-Holocene times in northern Australia. Nature 317, 711–713. https://doi.org/10.1038/317711a0

Woodroffe, S.A., Long, A.J., Punwong, P., Selby, K., Bryant, C.L., Marchant, R., Bronk Ramsey, C., Buck, C.E., Burr, G.S., Edwards, R.L., Friedrich, M., Grootes, P.M., Guilderson, T.P., Hajdas, I., Heaton, T.J., Hogg, A.G., Hughen, K.A., Kaiser, K.F., Kromer, B., McCormac, F.G., Manning, S.W., Reimer, R.W., Richards, D.A., Southon, J.R., Talamo, S., Turney, C.S.M., van der Plicht, J., Weyhenmeyer, C.E., 2015. Radiocarbon dating of mangrove sediments to constrain Holocene relative sea-level change on Zanzibar in the southwest Indian Ocean. The Holocene 25, 820–831. https://doi.org/10.1177/0959683615571422

Xu, Q., Tian, F., Bunting, M.J., Li, Y., Ding, W., Cao, X., He, Z., 2012. Pollen source areas of lakes with inflowing rivers: modern pollen influx data from Lake Baiyangdian, China. Quat. Sci. Rev. 37, 81–91. https://doi.org/10.1016/j.quascirev.2012.01.019

Yao, Q., Liu, K., 2017. Dynamics of marsh-mangrove ecotone since the mid-Holocene: A palynological study of mangrove encroachment and sea level rise in the Shark River Estuary, Florida. PLoS One 12, e0173670. https://doi.org/10.1371/journal.pone.0173670

Yao, Q., Liu, K. biu, Aragón-Moreno, A.A., Rodrigues, E., Xu, Y.J., Lam, N.S., 2020. A 5200-year paleoecological and geochemical record of coastal environmental changes and shoreline fluctuations in southwestern Louisiana: Implications for coastal sustainability. Geomorphology 365, 107284. https://doi.org/10.1016/j.geomorph.2020.107284

Yao, Q., Liu, K., Platt, W.J., Rivera-Monroy, V.H., 2015. Palynological reconstruction of environmental changes in coastal wetlands of the Florida Everglades since the mid-Holocene. Quat. Res. 83, 449–458. https://doi.org/10.1016/j.yqres.2015.03.005

Yao, Q., Liu, K., Ryu, J., 2018. Multi-proxy Characterization of Hurricanes Rita and Ike Storm Deposits in the Rockefeller Wildlife Refuge, Southwestern Louisiana. J. Coast. Res. 85, 841–845. https://doi.org/10.2112/si85-169.1

Zalasiewicz, J., Waters, C.N., Williams, M., Summerhayes, C., 2018. The Anthropocene as a Geological Time Unit: A Guide to the Scientific Evidence and Current Debate. Cambridge University Press.

Figure captions

Figure 1- a) Location of the study area, b) vegetation map with a stratigraphic profile (a`-b`) exhibiting vegetation, geomorphology, and the facies associations, c) drone image showing the coring sites along a sandy coastal barrier.,

Figure 2- Stratigraphy of core BC81 exhibiting sedimentary characteristics, facies associations, and pollen data with percentages of the ecological groups. Pollen diagrams are presented as percentages of the total pollen sum.

Figure 3- Stratigraphy of core BC82 exhibiting sedimentary characteristics, facies associations, and pollen data with percentages of the ecological groups. Pollen diagrams are presented as percentages of the total pollen sum.

Figure 4- Summary of core BC81, presenting sedimentary characteristics, pollen ecological groups, and geochemical data.

Figure 5- Summary of core BC82, presenting sedimentary characteristics, pollen ecological groups, and geochemical data.

Figure 6- Binary diagram showing the source of the sedimentary organic matter for each sedimentary facies associations based on the relationship between $\delta^{13}C$ and C/N.

Figure 7. Model of the geomorphology and vegetation development under the Holocene relative sea-level rise.

1352 Figure 8. American mangrove distribution in the tropical and subtropical zones and time
1353 of the mangrove establishment during the Holocene. The modern American mangrove
1354 distribution was obtained at http://data.unep-wcmc.org/datasets/4.

1355

1356 Table 1. Samples of sedimentary organic matter selected for radiocarbon dating and
1357 results with code site, laboratory number, depth (m), ^{14}C ages (yr BP, 1σ), calibrated
1358 ages (cal. yr BP, 2σ deviation), sedimentation rate and median of calibrated ages (cal. yr
1359 BP).
1360 Table 2. Characteristics of the three facies association.

1361

1362 Supplementary material

1363 Figure 1. Optical microscope photographs of *Typha* species with pollen in monad (a-b:
1364 *Typha angustifolia*) and tetrad (c-d: *Typha latifolia*).

1365

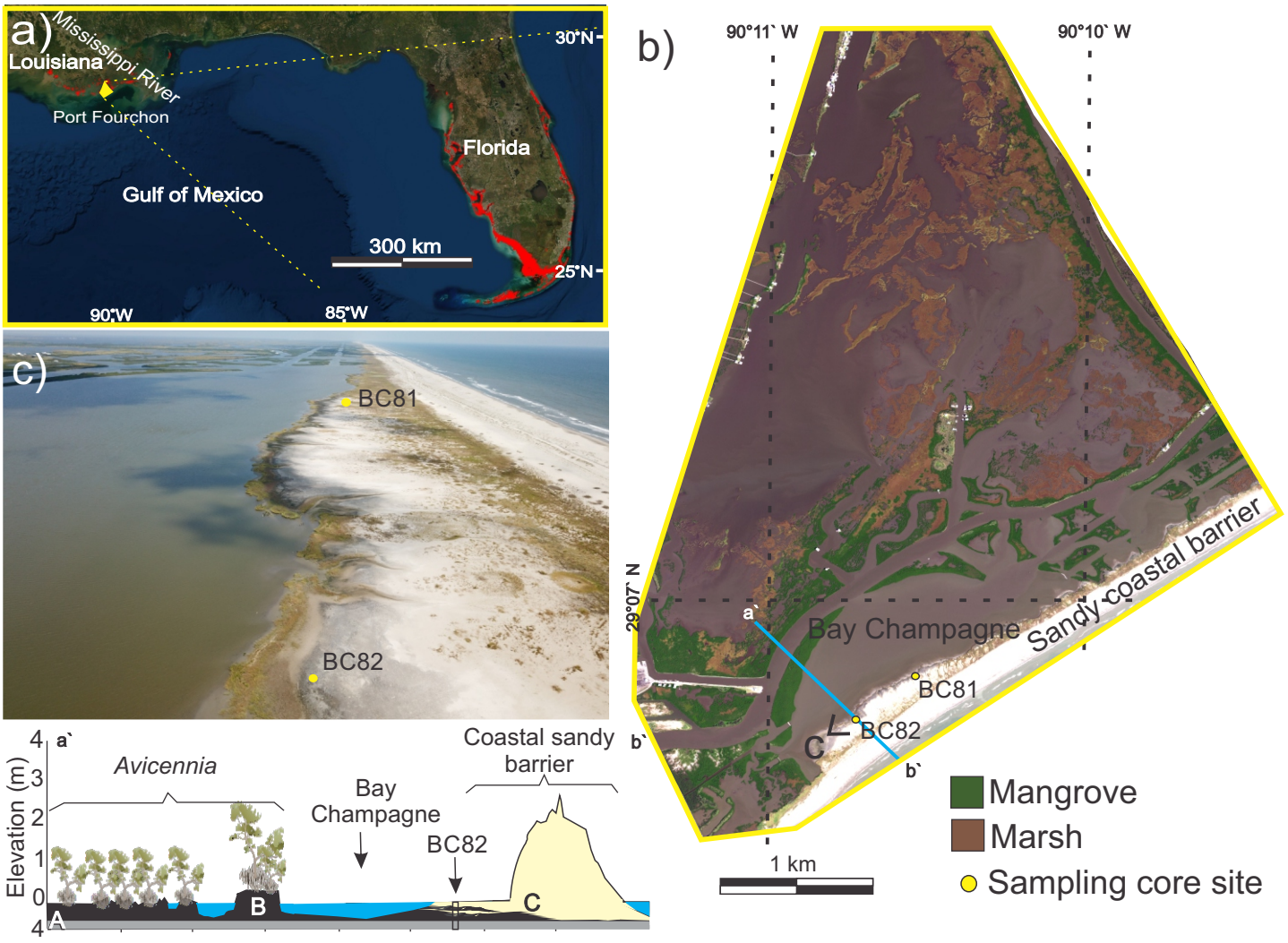
a)
Louisiana
Mississippi River
Port Fourchon
Gulf of Mexico
Florida
30°N
25°N
90°W
85°W
300 km
b)
90°11` W
90°10` W
29°07` N
a`
b`
Bay Champagne
Sandy coastal barrier
BC81
BC82
C
1 km
Mangrove
Marsh
Sampling core site
c)
BC81
BC82
Elevation (m)
4
3
2
1
0
4
a`
b`
Avicennia
Bay Champagne
Coastal sandy barrier
BC82
A
B
C

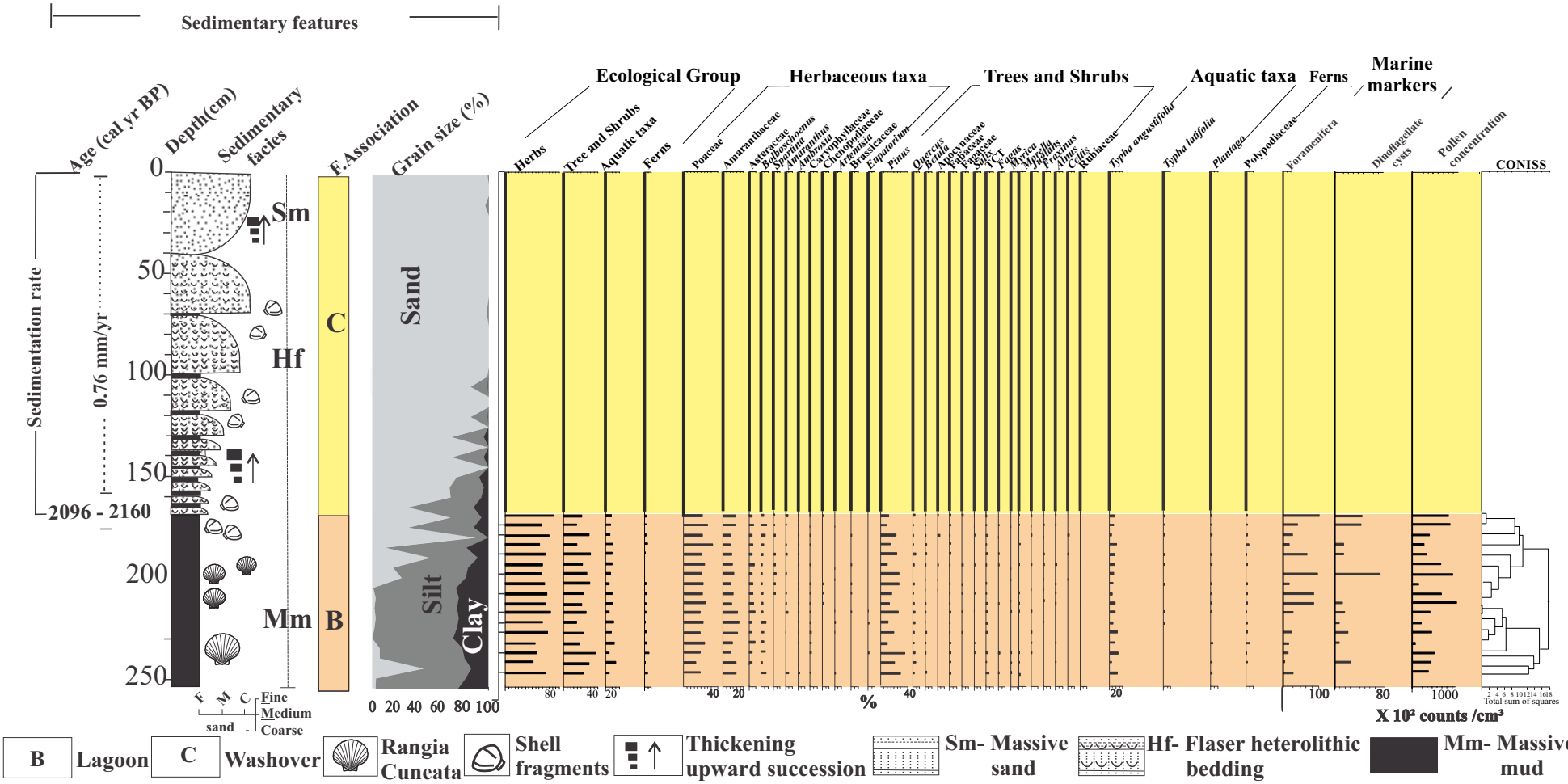
Sedimentary features
Ecological Group
Herbaceous taxa
Trees and Shrubs
Aquatic taxa
Ferns
Marine markers
Age (cal yr BP)
Depth(cm)
Sedimentary facies
F.Association
Grain size (%)
Herbs
Tree and Shrubs
Aquatic taxa
Ferns
Poaceae
Amaranthaceae
Asteraceae
Bolboschoenus
Sparganium
Amaranthus
Ambrosia
Caryophyllaceae
Chenopodiaceae
Artemisia
Brassicaceae
Eupatorium
Pinus
Quercus
Betula
Alnus
Fagaceae
Salix
Ulmus
Fraxinus
Tilia
Myrica
Fagus
Corylus
Rubiaceae
Typha angustifolia
Typha latifolia
Plantago
Polypodiaceae
Foraminifera
Dinoflagellate cysts
Pollen concentration
CONISS
Sedimentation rate
0.76 mm/yr
2096 - 2160
Sm
Hf
Mm
C
B
Sand
Silt
Clay
F M C
Fine
Medium
Coarse
sand
0 20 40 60 80 100
%
X 10² counts /cm³
Total sum of squares
B Lagoon
C Washover
Rangia Cuneata
Shell fragments
Thickening upward succession
Sm- Massive sand
Hf- Flaser heterolithic bedding
Mm- Massive mud

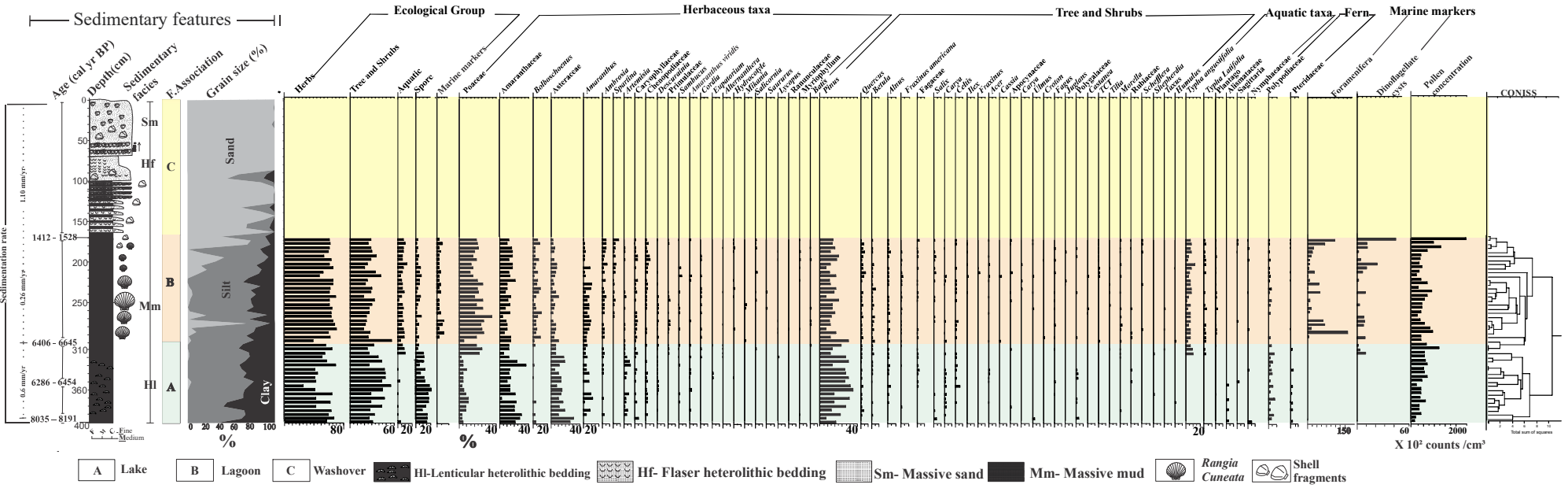
Sedimentary features
Ecological Group
Herbaceous taxa
Tree and Shrubs
Aquatic taxa
Fern
Marine markers
Age (cal yr BP)
Depth(cm)
Sedimentary facies
F.Association
Grain size (%)
Sedimentation rate
1.10 mm/yr
0.26 mm/yr
0.6 mm/yr
Sm
Hf
Mm
Hl
C
B
A
Sand
Silt
Clay
Fine
Medium
1412 - 1528
6406 - 6645
6286 - 6454
8035 - 8191
Herbs
Tree and Shrubs
Aquatic
Spore
Marine markers
Poaceae
Amaranthaceae
Bolboschoenus
Asteraceae
Amaranthus
Ambrosia
Spartina
Artemisia
Caryophyllaceae
Chenopodiaceae
Descurainia
Rumex
Ranunculus
Amaranthus viridis
Cerdia
Cuperaceae
Alternanthera
Helianthemum
Hydrocotyle
Malvaceae
Solidago
Taraxacum
Urtica
Ranunculaceae
Myriophyllum
Salix
Pinus
Quercus
Betula
Alnus
Fraxinus americana
Fagaceae
Salix
Carya
Celtis
Ilex
Fraxinus
Acer
Cassia
Apocynaceae
Carya
Ulmus
Croton
Fagus
Juglans
Polygalaceae
Castanea
CCTilia
Morella
Rubiaceae
Schaffera
Sloetherdia
Taxus
Rumex
Typha angustifolia
Typha Latifolia
Plantago
Sagittaria
Nymphaeaceae
Polypodiaceae
Pteridaceae
Foraminifera
Dinoflagellate cysts
Pollen concentration
CONISS
X 10² counts /cm³
A Lake
B Lagoon
C Washover
Hl-Lenticular heterolithic bedding
Hf- Flaser heterolithic bedding
Sm- Massive sand
Mm- Massive mud
Rangia Cuneata
Shell fragments

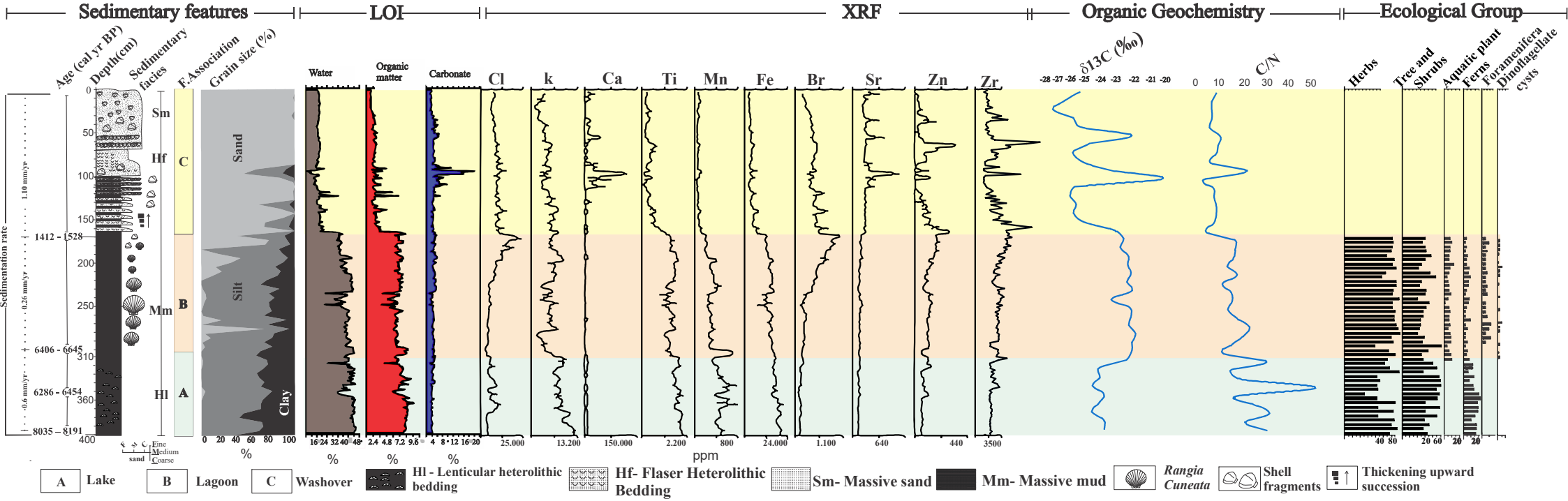
Sedimentary features
LOI
XRF
Organic Geochemistry
Ecological Group
Age (cal yr BP)
Depth(cm)
Sedimentary facies
F.Association
Grain size (%)
Water
Organic matter
Carbonate
Cl
k
Ca
Ti
Mn
Fe
Br
Sr
Zn
Zr
δ13C (‰)
C/N
Herbs
Tree and Shrubs
Aquatic plant
Ferns
Foramenifera
Dinoflagellate cysts
Sedimentation rate
1.10 mm/yr
0.26 mm/yr
0.6 mm/yr
1412 - 1528
6406 - 6645
6286 - 6454
8035 – 8191
Sm
Hf
Mm
Hl
A
B
C
Sand
Silt
Clay
Fine
Medium
Coarse
sand
%
ppm
A Lake
B Lagoon
C Washover
Hl - Lenticular heterolithic bedding
Hf- Flaser Heterolithic Bedding
Sm- Massive sand
Mm- Massive mud
Rangia Cuneata
Shell fragments
Thickening upward succession

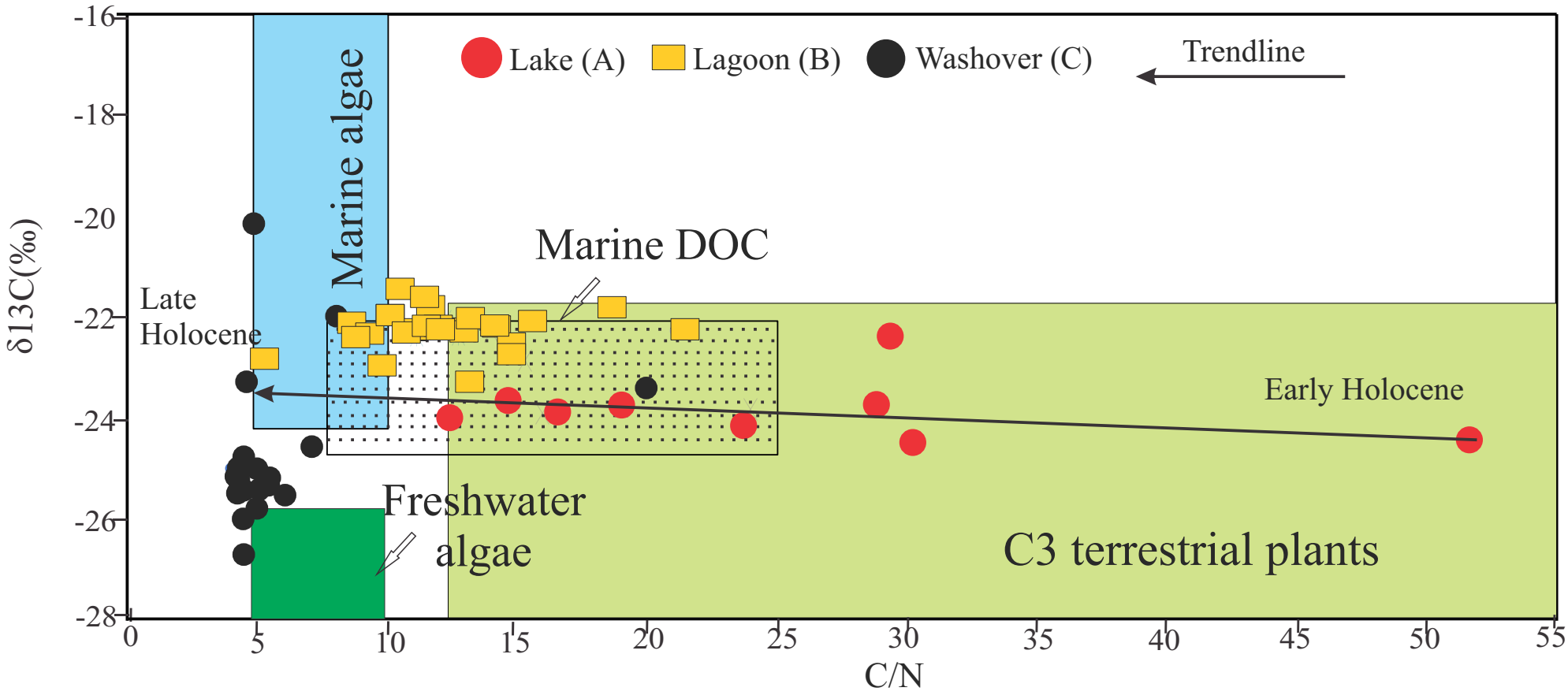
Lake (A)
Lagoon (B)
Washover (C)
Trendline
Marine algae
Marine DOC
Late Holocene
Early Holocene
Freshwater algae
C3 terrestrial plants
δ13C(‰)
C/N
-16
-18
-20
-22
-24
-26
-28
0
5
10
15
20
25
30
35
40
45
50
55

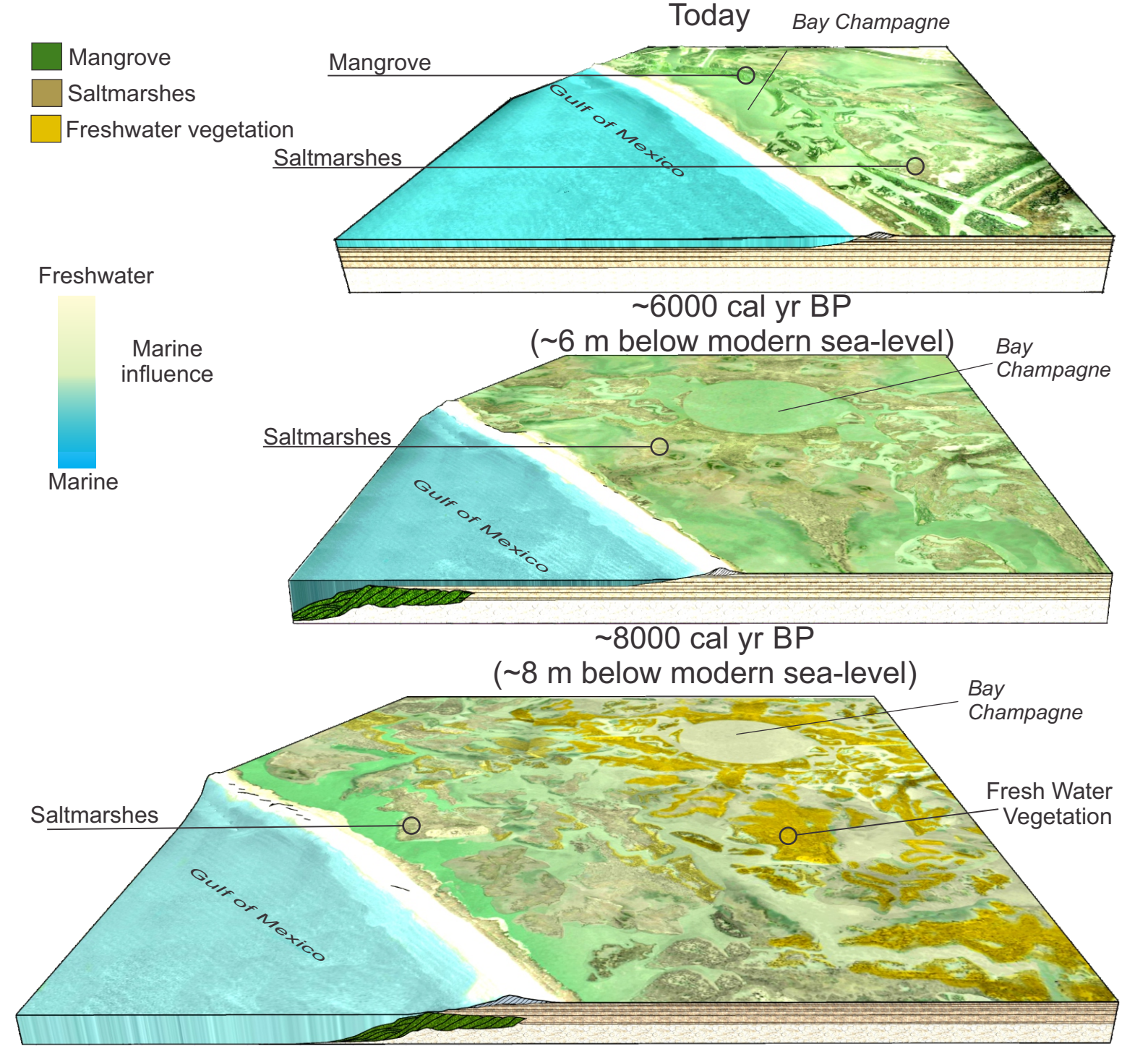
Today
Bay Champagne
Mangrove
Saltmarshes
Freshwater vegetation
Mangrove
Gulf of Mexico
Saltmarshes
Freshwater
Marine influence
Marine
~6000 cal yr BP
(~6 m below modern sea-level)
Bay Champagne
Saltmarshes
Gulf of Mexico
~8000 cal yr BP
(~8 m below modern sea-level)
Bay Champagne
Fresh Water Vegetation
Saltmarshes
Gulf of Mexico

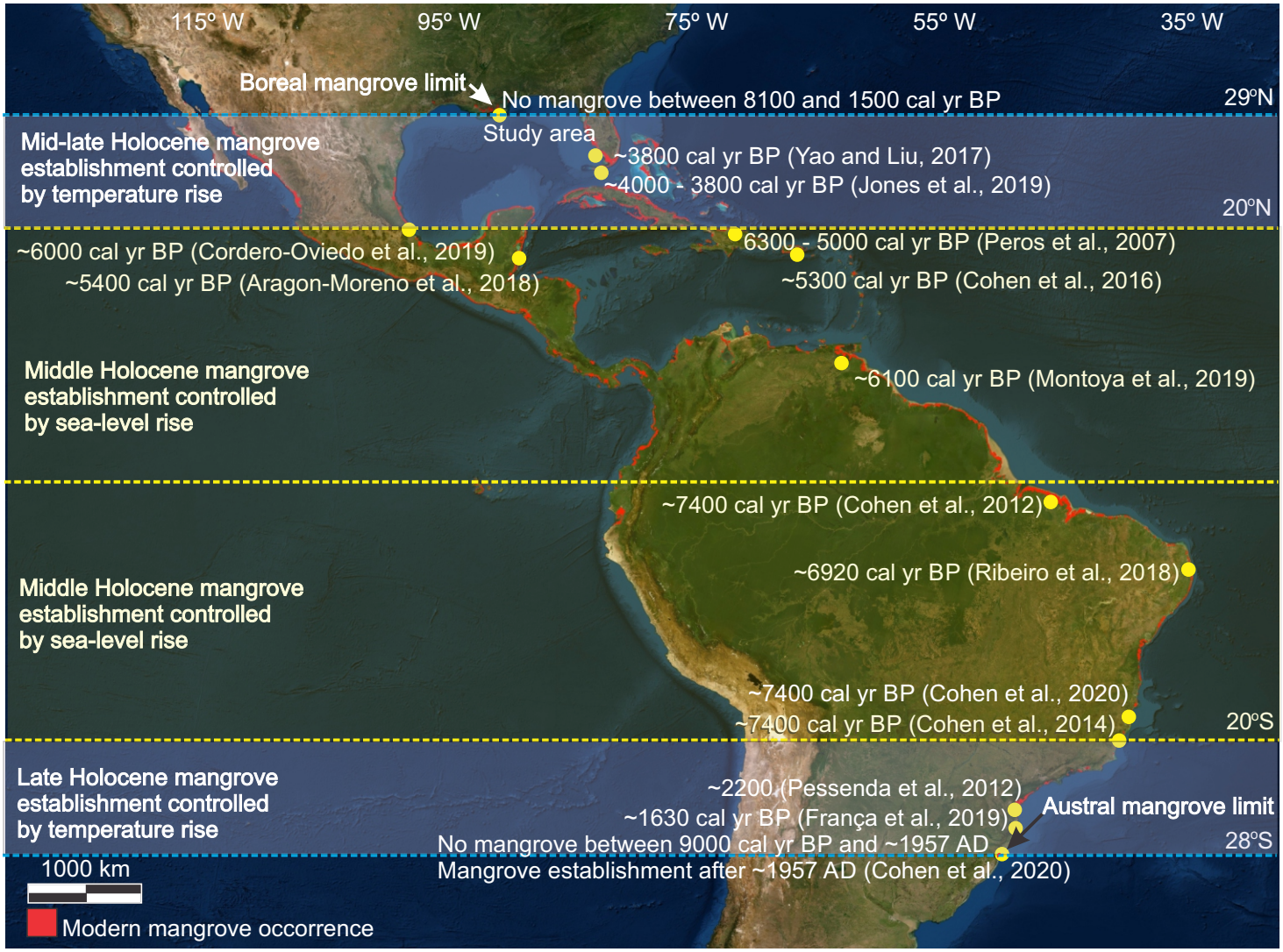
115° W
95° W
75° W
55° W
35° W
Boreal mangrove limit
No mangrove between 8100 and 1500 cal yr BP
29°N
Study area
Mid-late Holocene mangrove establishment controlled by temperature rise
~3800 cal yr BP (Yao and Liu, 2017)
~4000 - 3800 cal yr BP (Jones et al., 2019)
20°N
~6000 cal yr BP (Cordero-Oviedo et al., 2019)
~5400 cal yr BP (Aragon-Moreno et al., 2018)
6300 - 5000 cal yr BP (Peros et al., 2007)
~5300 cal yr BP (Cohen et al., 2016)
Middle Holocene mangrove establishment controlled by sea-level rise
~6100 cal yr BP (Montoya et al., 2019)
~7400 cal yr BP (Cohen et al., 2012)
~6920 cal yr BP (Ribeiro et al., 2018)
Middle Holocene mangrove establishment controlled by sea-level rise
~7400 cal yr BP (Cohen et al., 2020)
~7400 cal yr BP (Cohen et al., 2014)
20°S
Late Holocene mangrove establishment controlled by temperature rise
~2200 (Pessenda et al., 2012)
~1630 cal yr BP (França et al., 2019)
Austral mangrove limit
No mangrove between 9000 cal yr BP and ~1957 AD
28°S
Mangrove establishment after ~1957 AD (Cohen et al., 2020)
1000 km
Modern mangrove occorrence

Sediment core	Code site and laboratory number	Depth (m)	Ages (^{14}C yr BP, 1σ)	Ages (cal. yr BP, 2σ deviation)	Sedimentation rate (mm/yr)	Median of calibrated ages (cal. yr BP)
BC81	UGAMS-34381	170	2150±20	2096 - 2160	0.76	2128
BC82	UGAMS-34379	170	1580±20	1412 - 1528	1.1	1470
BC82	LAC 190456	300	5766±48	6406 - 6645	0.26	6525
BC82	LAC 190457	350	5621±48	6286 -6454-		6370
BC82	UGAMS-34380	400	7330±30	8035 – 8191	0.6	8113

Facies association	Facies description	Ecological group	Geochemical data	Elements predominance (ppm)	Interpretation
A	Lenticular heterolithic bedding (facies Hl)	Herbs, tree/shrubs, and ferns	$\delta^{13}C$= -24.4 − -22‰ C/N= 12 − 52	Fe: 14 k – 20 k K: 8 k – 13 k Ti: 1.5 k – 2 k Mn: 370 – 800	Lake
B	Massive mud (facies Mm) with *Rangia cuneate*	Herbs and aquatic plants from brackishwater. Foramenifera/ Dinoflagellate	$\delta^{13}C$= -23 − -21‰ C/N= 6 − 22	Cl: 3 k – 20 k Br: 190 – 950 Fe: 7 k − 17.5 k Mn: 186 – 500	Lagoon
C	Flaser heterolithic bedding (Hf), Massive sand (Sm) with shell fragments	No pollen/ferns	$\delta^{13}C$= -27 − -20‰ C/N= 5 − 20	Cl: 6 k – 24 k Ca: 2.7 k – 130 k Br: 230 - 1200 Sr: 100 – 572 Zr: 44 – 422	Washover